AMERICAN SOCIETY FOR MICROBIOLOGY | Molecular and Cellular Biology®

RESEARCH ARTICLE

IreA Controls Endoplasmic Reticulum Stress-Induced Autophagy and Survival through Homeostasis Recovery

Eunice Domínguez-Martín,[a,b] Laura Ongay-Larios,[c] Laura Kawasaki,[b] Olivier Vincent,[a] Gerardo Coello,[d] Roberto Coria,[b] Ricardo Escalante[a]

[a]Instituto de Investigaciones Biomédicas Alberto Sols, Consejo Superior de Investigaciones Científicas-Universidad Autónoma de Madrid (CSIC-UAM), Madrid, Spain

[b]Departamento de Genética Molecular, Instituto de Fisiología Celular, Universidad Nacional Autónoma de México, México City, México

[c]Unidad de Biología Molecular, Instituto de Fisiología Celular, Universidad Nacional Autónoma de México, México City, México

[d]Unidad de Cómputo, Instituto de Fisiología Celular, Universidad Nacional Autónoma de México, México City, México

ABSTRACT The unfolded protein response (UPR) is an adaptive pathway that restores cellular homeostasis after endoplasmic reticulum (ER) stress. The ER-resident kinase/RNase Ire1 is the only UPR sensor conserved during evolution. Autophagy, a lysosomal degradative pathway, also contributes to the recovery of cell homeostasis after ER stress, but the interplay between these two pathways is still poorly understood. We describe the *Dictyostelium discoideum* ER stress response and characterize its single bona fide Ire1 orthologue, IreA. We found that tunicamycin (TN) triggers a gene-expression reprogramming that increases the protein folding capacity of the ER and alleviates ER protein load. Further, IreA is required for cell survival after TN-induced ER stress and is responsible for nearly 40% of the transcriptional changes induced by TN. The response of *Dictyostelium* cells to ER stress involves the combined activation of an IreA-dependent gene expression program and the autophagy pathway. These two pathways are independently activated in response to ER stress but, interestingly, autophagy requires IreA at a later stage for proper autophagosome formation. We propose that unresolved ER stress in cells lacking IreA causes structural alterations of the ER, leading to a late-stage blockade of autophagy clearance. This unexpected functional link may critically affect eukaryotic cell survival under ER stress.

KEYWORDS *Dictyostelium*, ER stress, autophagy

The endoplasmic reticulum (ER) is a membranous network where about one-third of the synthesized proteins are folded and modified (1); ER is also critical for calcium homeostasis and lipid biosynthesis (2). Conditions that perturb the ER homeostasis interfere with proper protein folding, leading to the accumulation of unfolded proteins in the ER lumen. These conditions, referred to as ER stress, may have detrimental consequences on cellular function. Thus, a highly regulated pathway known as the unfolded protein response (UPR) has evolved to restore ER homeostasis both by reducing the ER protein load and by reprogramming gene expression to increase the ER folding capacity (3, 4) and protein degradation (5–7).

The UPR is triggered by three ER stress sensor proteins in mammalian cells, Ire1 (inositol-requiring enzyme), ATF6 (activating transcription factor 6), and PERK (protein kinase RNA-like ER kinase) (8), but only Ire1 is highly conserved between species (9). Ire1 is a type I transmembrane ER-resident protein that contains a serine-threonine kinase and an endoribonuclease domain at the cytosolic C terminus and an N-terminal luminal

Received 9 March 2018 **Accepted** 1 April 2018

Accepted manuscript posted online 9 April 2018

Citation Domínguez-Martín E, Ongay-Larios L, Kawasaki L, Vincent O, Coello G, Coria R, Escalante R. 2018. IreA controls endoplasmic reticulum stress-induced autophagy and survival through homeostasis recovery. Mol Cell Biol 38:e00054-18. https://doi.org/10.1128/MCB.00054-18.

Address correspondence to Roberto Coria, rcoria@ifc.unam.mx, or Ricardo Escalante, rescalante@iib.uam.es.

domain that can sense the protein-folding environment in the ER (10, 11). Under ER stress, Ire1 undergoes transautophosphorylation and activation of its endoribonuclease domain, which mediates the cleavage of a noncanonical intron contained in the mRNA of a basic leucine zipper (bZIP) transcription factor (Xbp1 in humans and Hac1 in yeast and bzip60 in plants). This splicing allows the synthesis of a functional protein, which controls the expression of chaperones, protein glycosylation enzymes, and proteases, among many other stress-response-related proteins (12–17).

Protein degradation participate in restoring cellular homeostasis after ER stress, mainly by two mechanisms: (i) the ERAD (ER-associated degradation) pathway that involves the proteasome (18, 19) and (ii) macroautophagy (19–22). Macroautophagy (here referred to as autophagy) is a conserved degradation mechanism in which intracellular double-membrane vesicles, denoted autophagosomes, capture cytosolic cellular components and organelles and then fuse with lysosomes to deliver this material for degradation (23). Basal autophagy is important for maintaining cellular homeostasis and is highly induced as a starvation survival response (24, 25). Other stimuli such as oxidative stress (26), pressure changes (27), or infection (28) can also induce autophagy.

Many ER stress-inducing drugs elicit an autophagic response (29), but the corresponding signaling pathways have been only partially elucidated. The three main UPR signaling branches seem to play differential roles in ER stress-induced autophagy. Reports addressing ER stress in mammalian cells suggest that Ire1 is required for autophagy induction, while ATF6 and PERK seem to be dispensable for this process (30). On the other hand, both PERK and Ire1 have been found to be necessary for the upregulation of some autophagic genes after ER stress (31). In plant and mammalian cells Ire1-dependent autophagy induction after ER stress seems to depend on the kinase domain of this sensor protein (30, 32). Further, in mammalian cells it has been shown that Ire1 activates autophagy after ER stress through the c-Jun N-terminal kinase (JNK) pathway (30). Nevertheless, autophagy is also induced after ER stress in organisms where the JNK pathway is not conserved, such as plants, yeasts, and algae (32–34). Therefore, if Ire1 is involved in the ER stress-dependent autophagic response in these organisms, it might be regulating other JNK-independent autophagy-inducing pathways.

The extent to which autophagy contributes to cell survival under ER stress conditions has not been clearly established. Observations from *Arabidopsis thaliana* suggest that the absence of some autophagic genes decrease plant viability after ER stress (35), although similar studies in yeasts present contradictory results (21, 36). In the present study, we sought to address these questions by studying the link between autophagy and ER stress in the model organism *Dictyostelium discoideum*, a soil-living social ameba that feeds on bacteria and yeasts. When nutrients are scarce, about 100,000 *Dictyostelium* cells aggregate and enter a developmental program that culminates in the formation of a fruiting body. Autophagy-defective mutants in *Dictyostelium* exhibit aberrant developmental phenotypes (37, 38). Since the ER stress response was not previously described in this model, we wanted to characterize the *Dictyostelium* response to ER stress and study the role of its single IRE1 orthologue gene (*ireA*). We found that a fully functional IreA is essential for ER stress survival and for the regulation of a specific gene expression program. In addition, we observed that *Dictyostelium* cells also require autophagy induction to survive ER stress. Interestingly, IreA absence does not prevent the induction of autophagy upon ER stress but rather impairs this process at a later stage, likely due to the inability of IreA-depleted cells to restore the ER homeostasis. Our results probably reveal an ancient interplay between UPR and autophagy that shapes the ER stress response in this model organism.

RESULTS

ER stress induction in *Dictyostelium*. The ER stress response had not been previously described in *Dictyostelium*, so we first studied the effect of commonly used ER stress inducers. *Dictyostelium* cells were exposed to 2 μg/ml tunicamycin (TN), 1.5 mM

dithiothreitol (DTT), or 200 mM 2-deoxy-D-glucose (2-DOG). Serial dilutions of treated cells were spotted on an SM medium plate containing a lawn of *Klebsiella aerogenes* to test cell viability. This assay was adapted to *Dictyostelium* from the commonly used spot assay to test drug sensitivity in yeasts (39, 40). After TN treatment, *Dictyostelium* cells were not able to divide and were severely impaired in their growth in association with bacteria. On the other hand, little or no effect was seen after a treatment with 2-DOG or DTT (Fig. 1A). We also observed that cell morphology was specifically altered by the TN treatment, as treated cells became rounded and more refractile (Fig. 1B) and had reduced adherence to the plastic surface. It has been previously reported that in other organisms ER stress induces the expression of ER-resident chaperones and components of the endoplasmic reticulum-associated degradation (ERAD) pathway (41, 42). Therefore, we analyzed by Western blotting the effects of different treatments on the expression of the ER-resident chaperone Grp78/BiP (which we identified to be coded by the DDB_G0276445 gene in *Dictyostelium* [Table 1]) and of the ERAD protein CdcD (homologous to human VCP/p97 and yeast Cdc48) (43), both highly conserved in *Dictyostelium*. Grp78 detection was performed with an antibody raised against the human Grp78 orthologue. This antibody recognized three bands in *Dictyostelium* protein extracts. The heaviest protein detected with this antibody corresponds to the estimated molecular mass (72 kDa) of the primary sequence of *Dictyostelium* Grp78. We consider this protein the bona fide *Dictyostelium* Grp78. The other two bands recognized by this antibody could correspond to chaperones of the Hsc70 family, HspB and HspE, with estimated masses of 70 and 69 kDa, respectively, which under some conditions comigrate in the gel. To further confirm the specificity of the antibody, the *Dictyostelium* Grp78/BiP gene was expressed in bacteria. Analysis of bacterial extracts with the anti-Grp78 antibody allowed detection of the *Dictyostelium* Grp78 orthologue (data not shown).

As shown in Fig. 1C and D, only TN significantly increased the expression of Grp78 (band *a*) and CdcD, while the bands corresponding to Hsc70 chaperones (band *b*) remained unchanged. TN treatment increased by ~8-fold and ~3-fold the expression of Grp78 and CdcD, respectively (Fig. 1D); in contrast, DTT and 2-DOG did not have a significant effect on the expression of both proteins.

Dictyostelium cells were subjected to increasing concentrations of TN and a dose-dependent negative effect on viability was observed in serial dilution-spot assays (Fig. 1E). An increase in expression of CdcD and the ~72-kDa protein detected by the anti-Grp78 antibody was observed for all doses tested (Fig. 1F and G). However, a significant increase in both markers was only observed after 16 h of treatment with 2 μg/ml TN (Fig. 1H and I). In conclusion, TN induces ER stress and triggers a response, whereas 2-DOG and DTT have no effect at the concentrations tested. The absence of 2-DOG effect could be due to its poor internalization rate in *Dictyostelium* cells (44). We did not characterize further the effect of DTT since it also blocks the formation of disulfide bonds of cytosolic proteins, which can lead to the formation of protein aggregates that may interfere with autophagy.

Identification and subcellular localization of the UPR sensor protein IreA in *Dictyostelium*. To identify the components of the UPR in *Dictyostelium*, the sequences of human, yeast, and *A. thaliana* UPR proteins were used as the query at the dictyBase BLAST-P program. As shown in Table 1, a putative *Dictyostelium* Ire1 orthologue (DDB_G0267650, IreA) was identified with a high level of protein sequence similarity to known Ire1 orthologues. It must be pointed out that although IfkA and IfkB were considered PERK homologues by the program, they lack the typical transmembrane domain and have already been described as orthologues of Gcn2 (45, 46). *Dictyostelium ireA* codes for a 984-residue protein that contains a signal peptide within the first 26 residues, a transmembrane domain (residues 440 to 457), a serine/threonine kinase domain (residues 575 to 851), and a kinase extension nuclease (KEN) domain (residues 854 to 984) (Fig. 2A). The sequence identity between IreA and the human, *Saccharomyces cerevisiae*, and *A. thaliana* Ire1 orthologues is mainly restricted to the kinase and KEN domains, ranging from 20 to 70%, and these proteins share less or no sequence

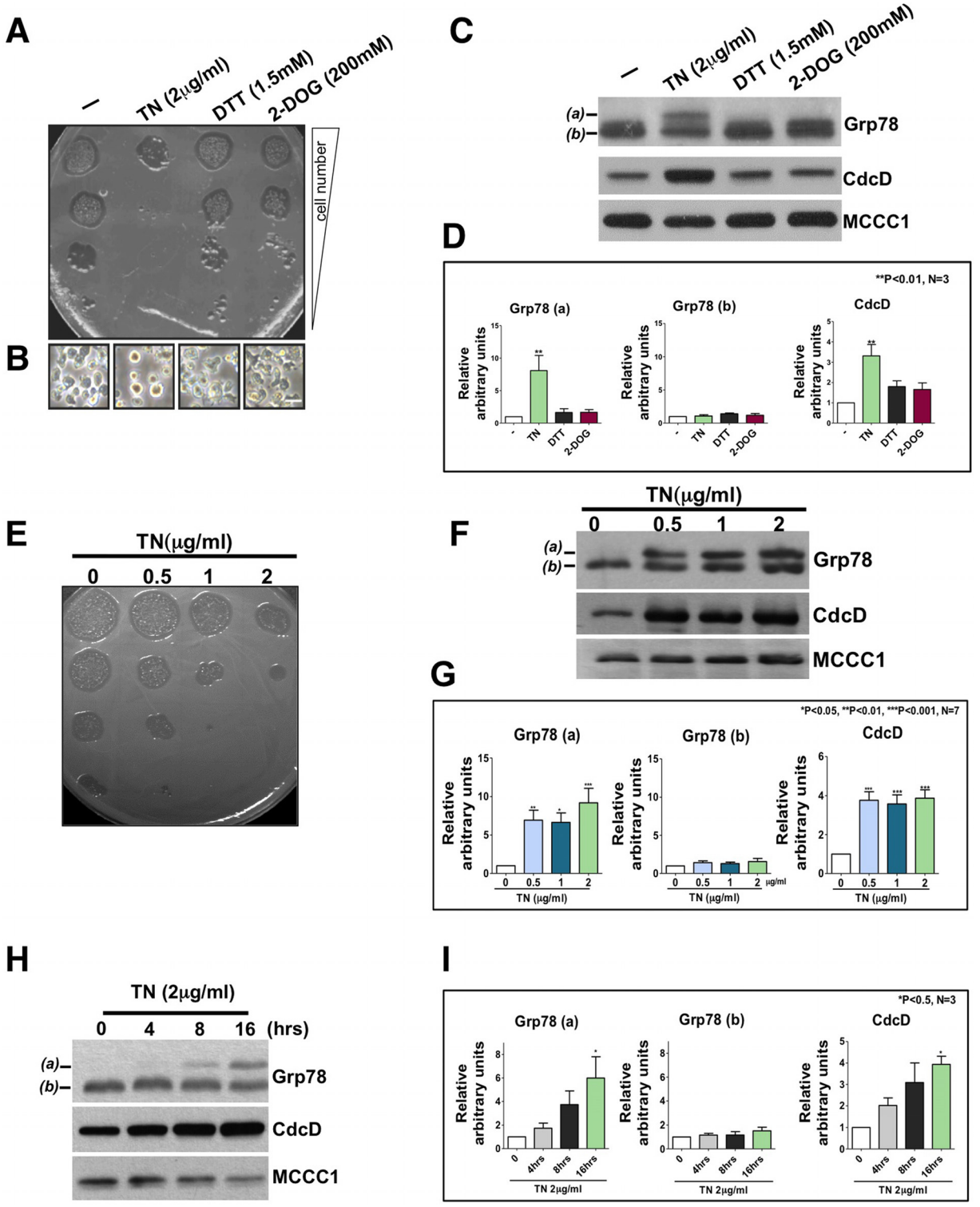

FIG 1 ER stress induction in *Dictyostelium*. (A) Cell viability of WT strain after 16 h of treatment with vehicle (DMSO), TN, DTT, or 2-DOG at the indicated concentrations. Cells were treated and spotted on SM plates containing a lawn of *K. aerogenes*, incubated at 22°C, and photographed 7 days later. (B) Phase-contrast microscopy from treated cells shown in panel A, taken right before the spot assay (scale bar, 10 μm). (C) Representative Western blot image of Grp78 and CdcD expression. (D) Densitometric quantification of Grp78 (bands a and b in panel C) and CdcD from cells treated as described in panel A. Bars represent the quotient of Grp78 or CdcD divided by MCCC1 and normalized with the DMSO treatment. Data are expressed as means ± the SD of three independent experiments. (E) Cell viability of WT strain after 16 h of treatment with different TN concentrations. Cells were treated as in panel A. (F) Representative Western blots of Grp78 and CdcD expression after different TN treatments. (G) Quantification was performed as for panel D. (H) Grp78 and CdcD expression after treatment with 2 μg/ml TN for the indicated times. Representative Western blot images are shown. (I) Quantification was performed as for panel D.

TABLE 1 BLAST analysis of *Dictyostelium* UPR orthologues

Query	UniProt identifier	Protein length(s) (spliced/unspliced [aa[a]])	*Dictyostelium* orthologue[b]	Protein length (aa)	e value
Xbp1/Hac1p	P17861 (XBP1_HUMAN)	261/376	ND		
	P41546 (HAC1_YEAST)	230/238			
	Q9C7S0 (BZP60_ARATH)	258/295			
Ire1p/Ern1	O75460 (ERN1_HUMAN)	977	IreA (DDB_G0267650)	984	4e–69
	P32361 (IRE1_YEAST)	1,115			1e–75
	Q93VJ2 (IRE1B_ARATH)	881			2e–78
BiP/Grp78/Kar2p	P11021 (GRP78_HUMAN)	654	DDB_G0276445	658	0
	P16474 (GRP78_YEAST)	682			0
	F4K007 (F4K007_ARATH)	613			0
Atf6	P18850 (ATF6A_HUMAN)	670	ND		
	Q9SG86 (BZP28_ARATH)	675	ND		
PERK	Q9NZJ5 (E2AK3_HUMAN)	1,116	IfkA (DDB_G0272837)*	2,258	4e–30
			IfkB (DDB_G0276829)*	1,358	2e–30

[a]aa, amino acids.
[b]*, IfkA and IfkB were previously described as GCN2 homologs (57, 94). ND, not detected.

similarity in the N-terminal sensor domain, located in the ER lumen (Fig. 2B). All of the Ire1 orthologues share a global sequence identity of about 30% (Fig. 2C).

To determine whether IreA, like its orthologues in other organisms (47), is an ER-resident protein in *Dictyostelium*, the predicted IreA coding sequence fused to green fluorescent protein (GFP) was introduced in *Dictyostelium* wild-type (WT) AX4 cells.

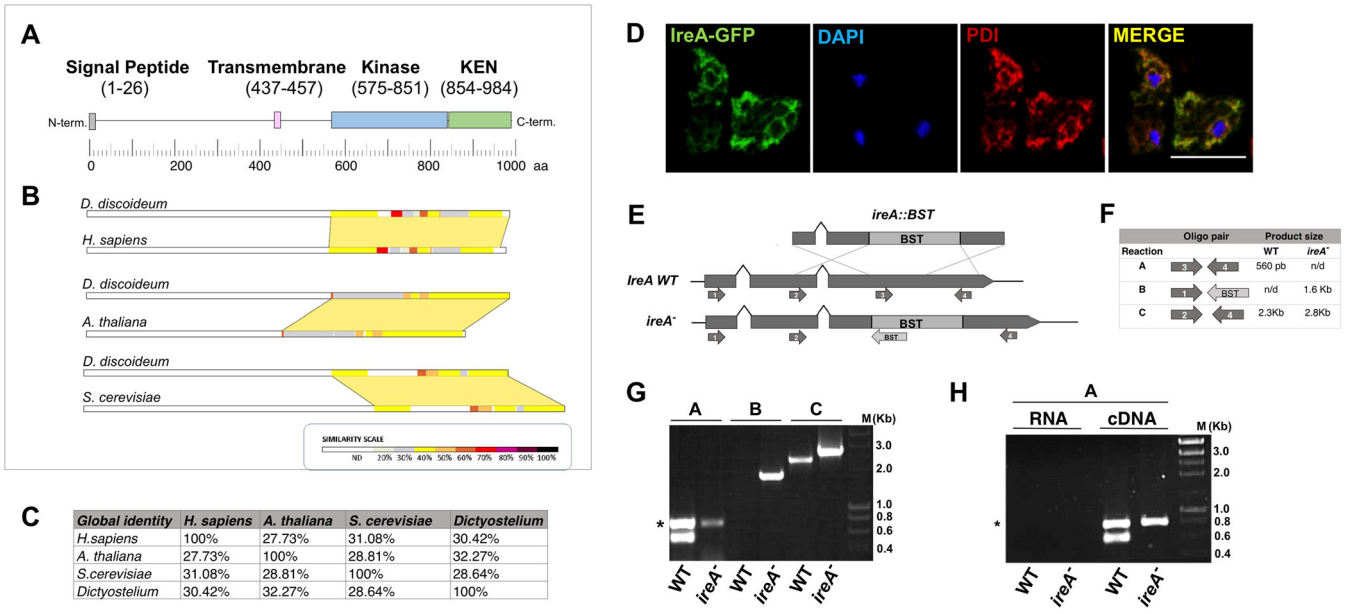

FIG 2 Sequence analysis of *Dictyostelium* IreA protein and its subcellular localization. (A) Diagram of the IreA predicted protein structure. The signal peptide (residues 1 to 26), the transmembrane region (residues 437 to 457), the kinase domain (residues 575 to 851), and kinase extension nuclease (KEN) domain (residues 854 to 984) are highlighted. (B) Pairwise alignments between *Dictyostelium* IreA and the *H. sapiens*, *A. thaliana*, and *S. cerevisiae* orthologues. Protein sequences of Ire1 orthologues were analyzed with SIM alignment tool, and results were visualized with LALNVIEW. (C) Percent identity between Ire1 orthologues obtained from a multiple alignment analysis. (D) Confocal microscopy of WT cells expressing an IreA-GFP hybrid protein, prepared for immunofluorescence detection of PDI (labeled with a secondary antibody conjugated to Alexa Fluor red 546) and DAPI-stained nuclei (scale bar, 10 μm). (E) Diagrams of the WT *ireA* locus, the *ireA*::BST construct, and the generated *ireA*$^-$ BST-interrupted locus. Gray boxes represent coding sequences; lines between boxes are introns. Arrows represent primers used for PCR amplification. A 998-bp deletion was generated in the *ireA* chromosomal locus by homologous recombination of a blasticidin (BST) resistance cassette. The insertion of BST in the *ireA* locus was corroborated by PCR with the indicated oligonucleotides. (F) Table presenting the expected sizes of the PCR amplification products that would be obtained with the respective oligonucleotide pairs depicted in panel E. (G and H) PCR products obtained using DNA (G) or cDNA (H) as the template. RNA was used as a negative control for DNA contamination. The asterisk denotes a control PCR amplification of an unrelated gene. M, molecular size marker.

Transformed cells were selected, fixed, and used for colocalization studies with the ER marker protein disulfide isomerase (PDI). IreA-GFP presented a reticulate pattern that clearly colocalized with PDI (Fig. 2D).

IreA-depleted cells cannot cope with ER stress. To study the function of IreA in *Dictyostelium*, the corresponding gene was deleted by inserting a blasticidin resistance cassette (BST) by homologous recombination (Fig. 2E). Several independent clones were obtained, and BST integration at the *ireA* locus was confirmed by genomic PCR (Fig. 2E to G). The lack of expression of a complete mRNA was also confirmed by reverse transcription-PCR (Fig. 2F and H). The *ireA*$^-$ mutant strains had no evident growth defects on liquid medium (HL5) or in association with bacteria. When development was analyzed, the only noticeable phenotype of this mutant was a slight delay in the culmination of some structures due to an extended period as migrating slugs (Fig. 3A). Nevertheless, normal-looking fruiting bodies were eventually formed.

We next sought to determine whether IreA is required for ER stress survival. For this, we analyzed the morphology of treated cells by microscopy after a 16-h TN treatment and observed that both WT and *ireA*$^-$ cells became rounded. Nevertheless, *ireA*$^-$ cells were much more affected, and some lysed cells were evident in the sample (Fig. 3B). Then, we evaluated whether *ireA*$^-$ cells could restore growth in association with bacteria after 4, 8, and 16 h of treatment with 2 μg/ml TN and found that *ireA*$^-$ cells grew poorly after all treatments (Fig. 3C).

Expression of the Grp78 chaperone was significantly decreased in the *ireA*$^-$ mutant in the presence of TN, dropping 4- to 5-fold with respect to its expression in the WT strain (Fig. 3D and E). Expression of CdcD showed exactly the same behavior as Grp78. This result indicates that the overexpression of both Grp78 and CdcD upon TN treatment is dependent on the presence of IreA. Together, these results indicate that *ireA*$^-$ cells are highly sensitive to TN and that IreA is required to cope with ER stress.

IreA kinase and RNase activities are both required for the ER stress response. We next examined the role of the putative IreA kinase and KEN domains in the *Dictyostelium* ER stress response by expressing WT and mutated forms of the IreA protein in the *ireA*-deficient strain and by determining the level of complementation of its TN-sensitive phenotype. A kinase-inactive mutant was generated by replacing a conserved lysine residue with asparagine (*ireA*^{K603N}) at the predicted ATP-binding site. The RNase-deficient mutant was generated by the substitution of a conserved asparagine in the KEN domain for alanine (*ireA*^{N927A}) (Fig. 4A). Both mutations have been proved to inactivate efficiently the kinase and RNase activities of Ire1 in other organisms (48, 49). The genes encoding the WT and mutant proteins tagged with GFP were introduced into the *ireA*$^-$ strain to determine their expression and cellular localization. As seen in Fig. 4B, the mutant proteins, as well as the wild-type protein, were distributed in a reticulated pattern characteristic of cortical and perinuclear ER and colocalized with the ER marker PDI. This indicates that both IreA mutant forms were expressed and inserted in the ER. We next sought to determine whether these mutant alleles could revert the ER stress response deficiency of the *ireA*$^-$ mutant. We found that the expression of both mutant genes did not allow the growth of the *ireA*$^-$ mutant after incubation with 2 μg/ml TN (Fig. 4C). The mutant proteins were also unable to induce expression of Grp78 and CdcD after the TN treatment (Fig. 4D and E). Overall, these results indicate that the ER stress response and the regulation of the expression of Grp78 and CdcD depend on both the kinase and the RNase activities of IreA.

It has been observed that yeast and human Ire1 form high-order oligomers during ER stress conditions (50). To assess whether *Dictyostelium* IreA can associate and form oligomers under stress and to evaluate whether the kinase and RNase activities are required in this process, we analyzed cells expressing the WT and mutant proteins tagged with GFP by live confocal imaging. TN treatment induced IreA association (cluster formation seen as tiny puncta) in approximately 30% of the cells in the *ireA*$^-$ strain expressing the IreA WT construct (Fig. 4F and G). This proportion remained constant until 8 h of treatment with TN (Fig. 4G). Interestingly, although mutant forms

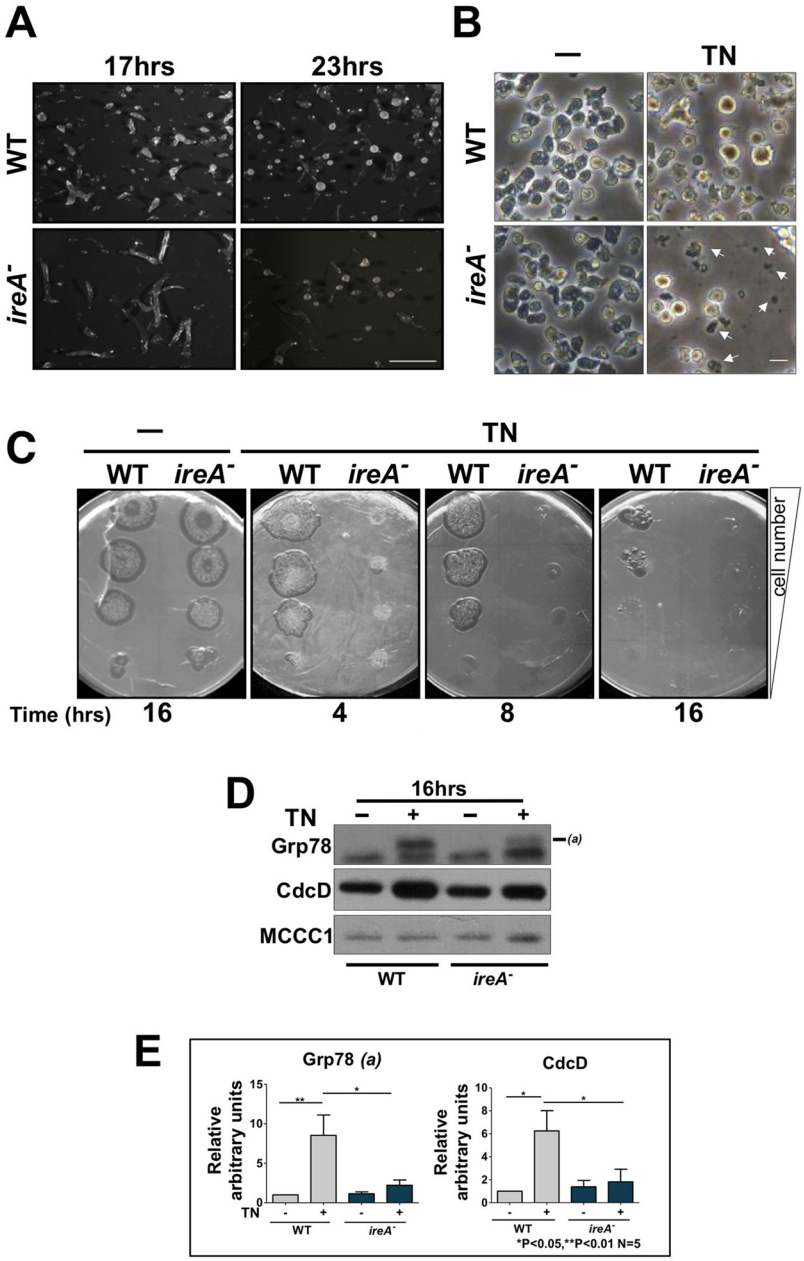

FIG 3 Effects of *ireA* inactivation on development and ER stress response. (A) Photographs of WT and *ireA*$^-$ strains showing different development stages (scale bar, 1 mm). Cells were deposited over nitrocellulose filters without nutrients and allowed to develop for the indicated times. (B) Light microscopy pictures of WT and *ireA*$^-$ cells treated for 16 h with vehicle (DMSO) or TN (2 μg/ml). Arrows point to lysed cells and debris (scale bar, 10 μm). (C) Serial dilution spot assay of WT and *ireA*$^-$ cells treated for the indicated times with vehicle (DMSO) or TN (2 μg/ml). (D and E) Representative Western blot (D) and densitometric quantification of Grp78 (*a*) and CdcC expression in WT and *ireA*$^-$ cells after 16 h of treatment with TN (2 μg/ml) (E). Densitometry was performed as described for Fig. 1D. Values are means $\pm$ the SD of five independent assays. Statistical significant differences are indicated by asterisks.

of IreA could oligomerize, the proportion of cells with clusters was significantly different from that observed in the WT. Around 15% of the cells expressing the kinase-inactive IreA mutant (*ireA*^{K603N}) presented cluster formation, while almost 100% of the RNase-inactive mutant (*ireA*^{N927A}) cells contained clusters (Fig. 4F and G). This indicates that the point mutations that inactivate either the kinase or the RNase activities do not affect IreA association but do alter the regulation and abundance of cluster structures.

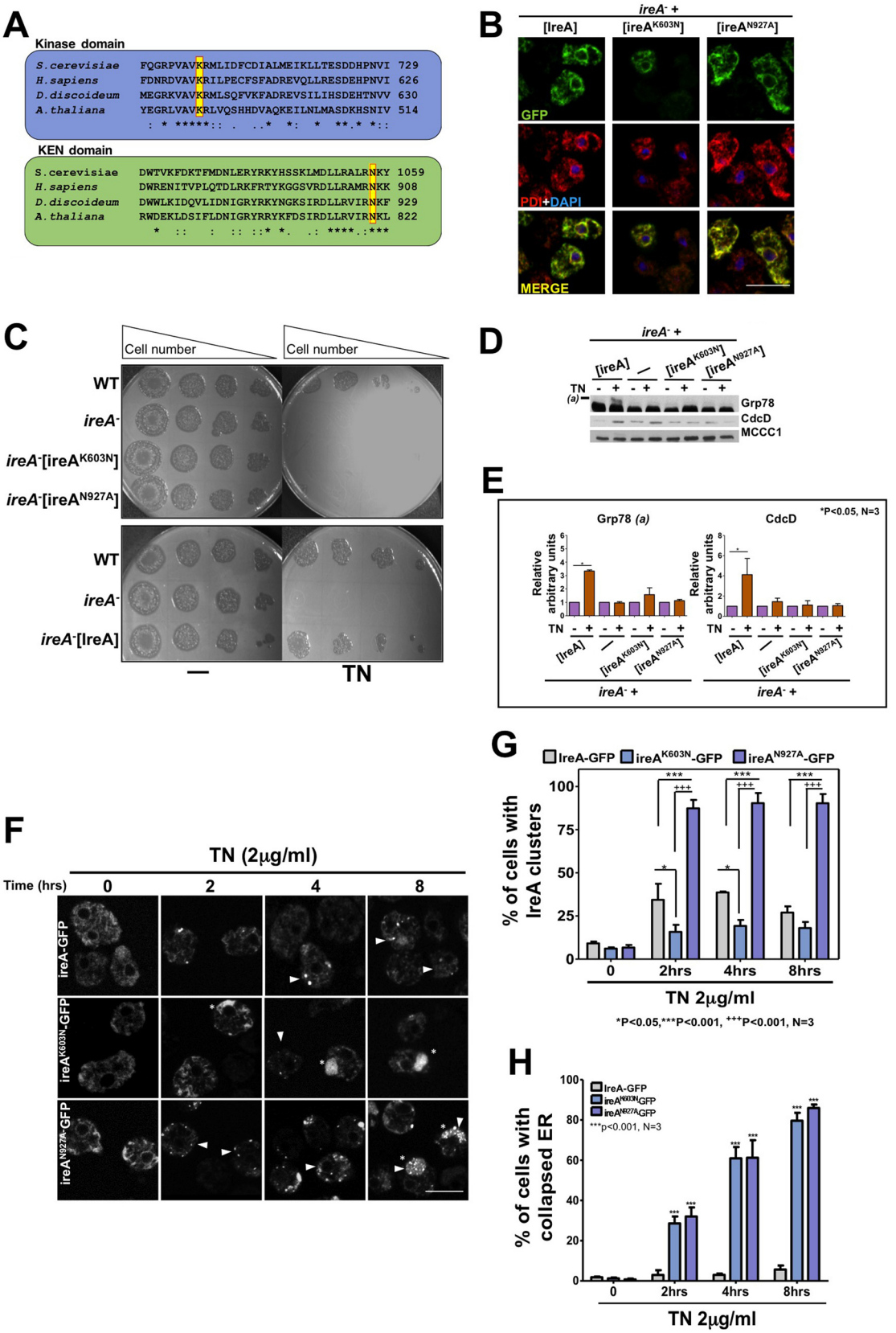

FIG 4 Effects of IreA kinase and KEN point mutations on ER stress response. (A) Alignment of the kinase and RNase domains of *S. cerevisiae*, *H. sapiens*, *D. discoideum*, and *A. thaliana* Ire1 orthologues. The conserved residues that were mutated on *D. discoideum* IreA are highlighted. K603 and N927 (relative to *D. discoideum*) were mutated to N and A, respectively. (B) Confocal microscopy of

(Continued on next page)

It has been observed that the morphology of the ER is altered during stressful conditions (21) and that ER cisternae can collapse in Ire1-defficient cells (51). Similar effects were observed in *Dictyostelium* cells after a TN treatment, and we thus determined ER damage during TN treatment in cells expressing either the WT or mutant IreA constructs. Some cells under TN treatment showed a large collapsed ER structure instead of a well-spread tubular ER (Fig. 4F). We quantified the percentage of cells with this aberrant ER by live confocal microscopy. The proportion of cells with collapsed ER increased significantly in cells expressing IreA-mutant versions (Fig. 4H) compared to that of the WT in a time-dependent manner. After 8 h of TN treatment, most cells expressing IreA mutant forms presented a collapsed ER, while the cells expressing the WT version maintained a normal ER morphology. Taken together, these results suggest that in order to maintain the integrity of the ER during stress conditions, the cells require both the kinase and RNase activities of IreA and that this process is independent on the capacity to form oligomeric IreA structures.

IreA participates in a TN-induced transcriptional response. In *S. cerevisiae* and other organisms, the ER stress response triggers a gene expression program regulated by Ire1 through the activation of a b-zip transcription factor (7), whereas in some species the ER stress does not induce a transcriptional reprogramming; instead, the response relies on the regulation of mRNAs stability (52). To gain insight into the transcriptional changes that TN treatment elicit in *Dictyostelium* cells and to assess whether IreA is implicated in this response, we performed deep RNA sequencing of poly(A) RNA extracted from WT and *ireA*$^-$ cells treated with 2 μg/ml of this drug or with the vehicle (dimethyl sulfoxide [DMSO]). In WT cells, we observed that 433 transcripts were differentially regulated after a TN treatment. Within this group, 166 transcripts were upregulated ($\log_2$ fold change $\geq$ 1.3) (Fig. 5A; see also Archive S1 in the supplemental material), whereas 267 were downregulated ($\log_2$ fold change ≤ -1.3) (Fig. 5B; see also Archive S1 in the supplemental material). From these data, we estimated that the transcript levels of nearly 3.5% of *Dictyostelium* genes were altered after a TN treatment. The participation of IreA in the transcriptional response elicited by TN was evaluated by obtaining the set of genes whose expression change depended on IreA. We found that 76 of the 166 genes that were upregulated and 92 of the 267 genes that were downregulated by a TN treatment in the WT strain were IreA dependent (Fig. 5A and E; see also Archive S2 in the supplemental material).

To determine which processes might be affected after a TN treatment, we categorized the up- and downregulated sets of genes using the DAVID gene ontology (GO) enrichment clustering tool (53, 54). For this analysis, we used the default parameters of the program and selected the categories "biological process," "protein domain," and "cellular component." The clusters resulting from the enrichment analysis are briefly displayed in Fig. 5, and the complete results are available in Archives S3 and S4 in the supplemental material. This clustering analysis revealed that the upregulated set of genes is associated with the ER stress response (Fig. 5C) and is significantly enriched in terms related to protein degradation processes ("protein ubiquitination," "ubiquitin,"

FIG 4 Legend (Continued)
ireA$^-$ cells expressing WT IreA and its mutated versions (K603N and N927A) tagged with GFP. Cells were fixed and stained with DAPI, and PDI was immunodetected as in Fig. 2D (scale bar, 10 μm). (C) Serial dilution spot assay of *ireA*$^-$ cells expressing, an IreA-GFP, IreA^{K603N}-GFP, or IreA^{N927A}-GFP construct. Cells were treated for 16 h with vehicle (DMSO) or TN (2 μg/ml), spotted over a lawn of *K. aerogenes*, and photographed 5 to 7 days later. (D and E) Representative Western blot and (D) densitometric quantification of Grp78 [(*a*)] and CdcD expression after a DMSO or TN (2 μg/ml) treatment of *ireA*$^-$ cells expressing either IreA-GFP, IreA^{K603N}-GFP, or IreA^{N927A}-GFP (E). Densitometry was performed as described for Fig. 1D. Values are the means $\pm$ the SD of three independent assays. Asterisks indicate statistically significant differences. (F) One-stack confocal microscopy images of the localization and clustering (formation of puncta) of IreA-GFP, IreA^{K603N}-GFP, and IreA^{N927A}-GFP. *ireA*$^-$ cells expressing the fusion proteins were treated with TN (2 μg/ml) for the indicated times. *In vivo* confocal images were taken every 2 h (scale bar, 10 μm). Arrowheads indicate cells containing IreA clusters, and asterisks indicate cells presenting collapsed ER. (G) Percentage of cells containing IreA clusters. Values represent the means $\pm$ the SD of three independent experiments. Statistically significant differences are denoted by an asterisk [between WT and mutant IreA(s)] and by a "+" sign (between *ireA*^{K603N} and *ireA*^{N927A}). (H) Percentage of *ireA*$^-$ cells presenting collapsed ER. Cells with collapsed ER (see panel F) were counted, and the mean percentages $\pm$ the SD of three independent experiments were graphed. Statistically significant differences relative to the DMSO treatment are indicated.

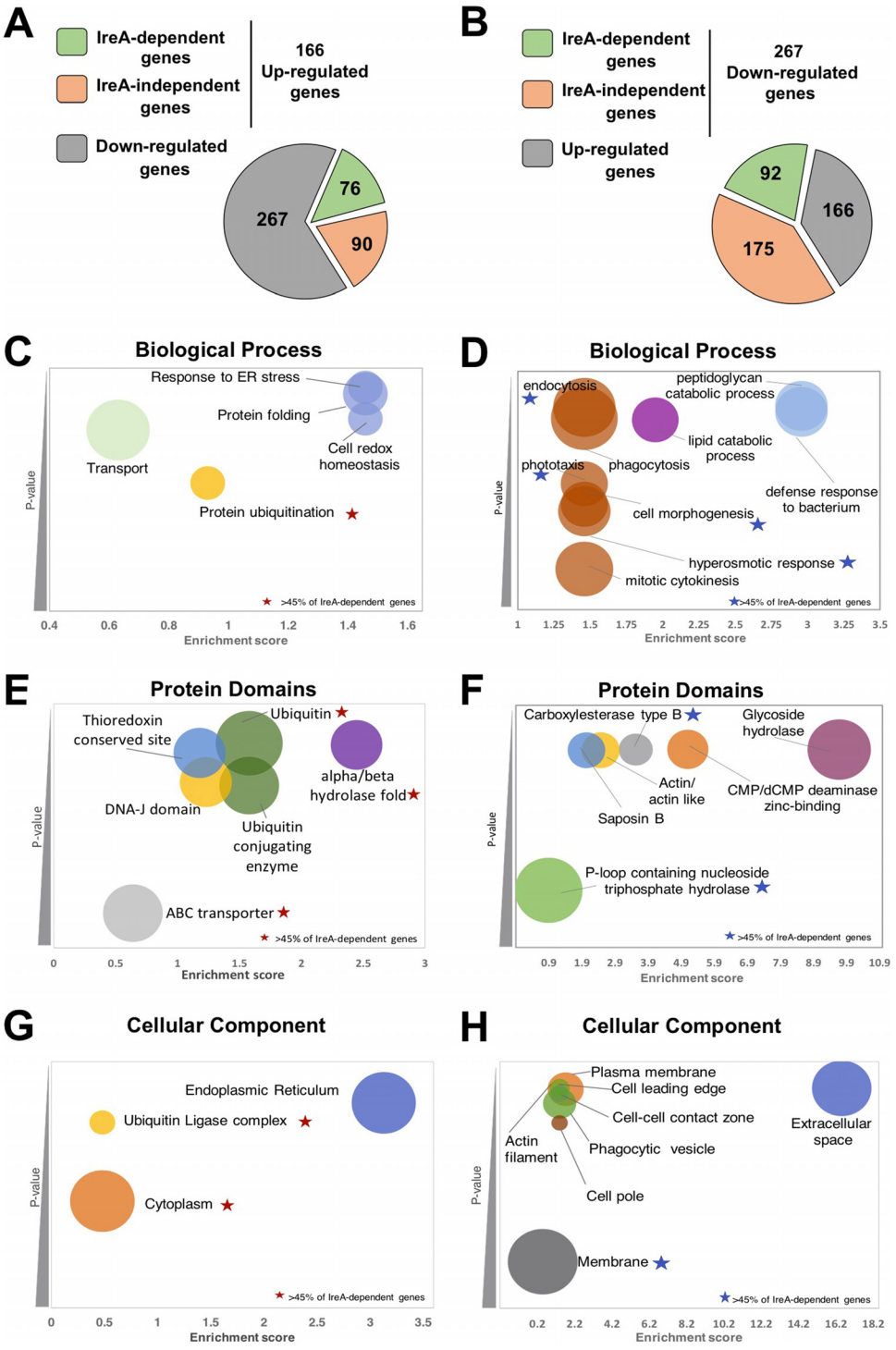

FIG 5 Identification of IreA-dependent and IreA-independent regulated genes upon TN treatment. RNA-seq was used to detect gene expression changes in WT and *ireA*$^{-}$ strains treated or not treated with TN (2 μg/ml). Only genes with a $\log_2$ fold change of $\geq$1.3 were included. (A and B) Upregulated (A) and downregulated (B) genes after TN treatment. Both upregulated and downregulated gene groups were analyzed with the DAVID gene ontology enrichment tool. (C to H) Genes were clustered into three categories for both upregulated genes (C, E, and G) and downregulated genes (D, F, and H): biological process (C and D), protein domains (E and F), and cellular component (G and H). The GO terms of the enriched clusters are presented in accordance with the obtained enrichment score and *P* value ($\geq$0.5), and the color code highlights GO terms that belong to the same cluster. The size of the bubble corresponds to the number of genes in each cluster. GO clusters where at least 45% of the genes were IreA dependent are indicated by stars.

"ubiquitin conjugating enzyme," and "alpha/beta hydrolase fold") and to protein folding ("DNA-J domain" and "thioredoxin containing site") (Fig. 5C, E and G; see also Archive S3 in the supplemental material). Also, from these results it can be inferred that TN could be upregulating transport-related processes (Fig. 5C and E).

In contrast, the GO cluster results of the downregulated set of genes were completely different (Fig. 5D, F, and H; see also Archive S4 in the supplemental material). "Carbohydrate metabolism" was the most enriched biological term for this set of genes, and "glycoside hydrolase" was the most enriched term in the protein domain category (Fig. 5D and F). These data suggest that *Dictyostelium* cells may experience an imbalance in the carbohydrate metabolism after a TN treatment, possibly caused by the effect of this antibiotic on protein glycosylation. Interestingly, the downregulated set is enriched in lipid metabolism terms (Fig. 5D; see also Archive S5 in the supplemental material). Since many of the proteins associated with lipid metabolism are targeted to the ER, this group of transcripts might be downregulated to alleviate ER protein load. Nevertheless, another group of genes associated with lipid metabolism is upregulated (see Archive S5 in the supplemental material), reflecting that lipid homeostasis might be adapted to cope with ER stress. The term "extracellular space" was significantly enriched in the downregulated set of genes (Fig. 5H), suggesting an effect on secreted proteins. In addition, many of the downregulated transcripts code for membrane proteins or proteins involved in processes that require membrane remodeling, such as endocytosis, phagocytosis, and hyperosmotic stress (Fig. 5D and H). These data suggest that in *Dictyostelium* one of the functions of the UPR may be to downregulate the expression of proteins that are targeted to the secretory pathway or that should be inserted into the membrane, possibly to alleviate the ER protein load.

From the set of genes that are upregulated after a TN treatment, we observed that the clusters related to protein degradation processes (such as protein ubiquitination, ubiquitin ligase complex, ubiquitin, and alpha/beta hydrolase fold) contains a higher percentage (more than 45%) of IreA-dependent genes (Fig. 5C, E, and G; see also Archive S1 in the supplemental material). This suggests that the IreA-dependent response might contribute significantly to increase the degradative capacity of the cell, mainly through ubiquitin-related processes. IreA may also be required to increase drug resistance, since it was required for the upregulation of two transcripts that code for multidrug resistance ABC transporters (*abcC5* and *abcG10*) (see Archive S3 in the supplemental material). In addition, almost all clusters related to biological processes that were obtained from the analysis of the downregulated set of the genes contained more than 45% of IreA-dependent genes (Fig 5D, F, and H), and most of them code for membrane proteins (Fig. 5H), suggesting that IreA might alleviate the ER protein load by decreasing the abundance of transcripts that code for membrane-localized proteins.

We observed that under nonstressful conditions, IreA regulates the transcription of only 25 genes (see Archive S6 in the supplemental material). In addition, the transcript level of a large subset of genes (1,988) was altered specifically in the *ireA*$^-$ mutant strain after a TN treatment. Since the absence of IreA during ER stress compromises cell viability and may have profound consequences in multiple cellular processes, these transcriptional changes might reflect a strong compensatory response related with cell survival and/or cell death-related pathways.

Altogether, these data strongly suggest that ER stress triggers a complex transcriptional response that modulates the levels of a diverse set of transcripts, increasing the expression of proteins involved in protein folding and degradation while decreasing the expression of proteins that may burden the ER capacity. Also, the fact that nearly half of the transcriptional response is mediated by IreA suggests that IreA might regulate the activity of an unknown transcription factor under ER stress conditions. Our data also suggest the existence of an IreA-independent pathway responsible for the regulation of the remaining transcriptional response observed in an *ireA*$^-$ mutant.

Autophagy contributes to cell survival under ER stress. Since autophagy in *Dictyostelium* is activated by a variety of stress conditions such as starvation and

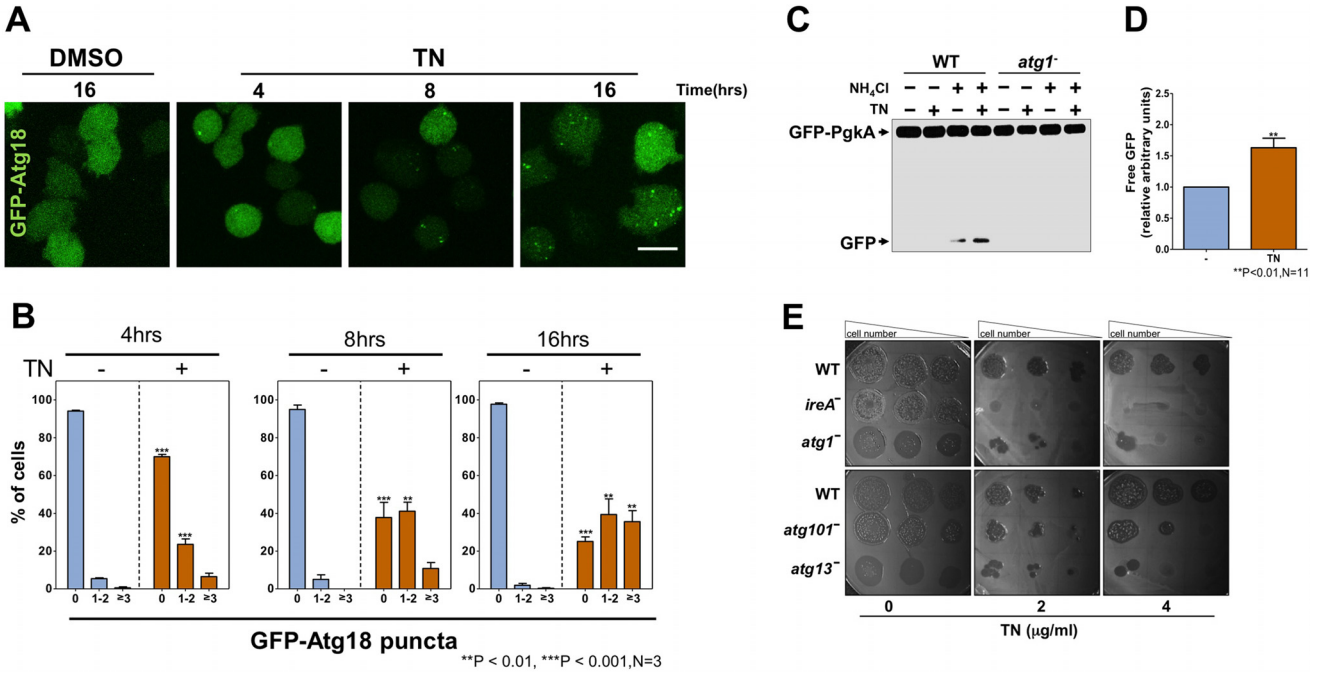

FIG 6 Tunicamycin induces autophagy. (A) Autophagy was determined as punctum formation in cells expressing GFP-Atg18 (maximum intensity z-projection representative picture). WT cells were treated with vehicle (DMSO) or TN (2 μg/ml) for the indicated times and visualized by confocal microscopy (scale bar, 10 μm). (B) Percentages of cells containing 0, 1 or 2, or ≥3 GFP-Atg18 puncta. Values are means ± the SD of three independent experiments. Asterisks indicate statistically significant differences. (C) Representative Western blot of an NH_4Cl-induced GFP-PgkA cleavage assay. WT and *atg1*⁻ cells overexpressing the GFP-PgkA were treated for 8 h with TN (2 μg/ml) or vehicle (DMSO). During the last 2 h of treatment, the cells were incubated in the presence or absence of NH_4Cl as described in Materials and Methods. (D) Quantification of accumulated free GFP in WT cells as determined by densitometry. GFP was normalized against GFP-PgkA and refers to DMSO-treated cells. The means ± the SD of 11 independent experiments were graphed. Asterisks denote significance. (E) Visualization of cell viability through a serial dilution spot assay. The indicated strains were treated for 16 h with TN or DMSO and spotted on a lawn of *K. aerogenes*. Plates were incubated at 22°C and photographed 5 to 7 days later.

mechanical stress (55), we next sought to characterize the autophagic response to ER stress by measuring autophagy induction in cells exposed to a TN treatment. Quantification of GFP-Atg18-positive puncta has been previously reported to be an accurate method to evaluate autophagy induction in *Dictyostelium* (56).

WT cells expressing GFP-Atg18 were treated for 4, 8, and 16 h with TN and analyzed *in vivo* by confocal microscopy (Fig. 6A). We observed that the TN treatment caused a significant increase in the autophagosome-containing cell population in a time-dependent manner (Fig. 6A and B), since the proportion of cells containing multiple GFP-Atg18 puncta increased with longer exposure to TN (Fig. 6B). We next sought to determine whether the increase in autophagosome formation induced by TN was associated with a higher degradative capacity. To answer this question, we measured the accumulation of free GFP derived from the cleavage of the cytosolic fusion protein PgkA-GFP in the presence of a nonsaturating NH_4Cl concentration. This protocol has been established to evaluate protein degradation associated with autophagy (57, 58). We found that TN treatment caused a significant increase in the accumulation of free GFP (Fig. 6C and D). This accumulation was detected after the addition of NH_4Cl only in the WT but not in the *atg1*⁻ strain, indicating that GFP-PgkA degradation is associated with the autophagy pathway.

We tested whether the autophagy pathway is required for a normal cellular response to TN. For this, we tested mutants of Atg1, Atg13, and Atg101 that block autophagy. The three proteins are constituents of the Atg1 complex but display different autophagy phenotypes. Atg1 and Atg13 are essential for autophagy induction, so knockout mutant strains present a complete autophagy blockage, whereas Atg101, which might play only a regulatory role, exhibits reduced levels of autophagy (59). All mutants were sensitive to TN treatment, although their sensitivity was not as

strong as that of the *ireA*$^-$ strain (Fig. 6E). As expected, both *atg1*$^-$ and *atg13*$^-$ strains appeared to be more sensitive to TN treatment than the *atg101*$^-$ strain. These results indicate that autophagy is part of the cellular response to TN and is required to trigger a complete response to ER stress.

IreA is dispensable for autophagy induction but is required for efficient autophagy. The autophagic response of *ireA*$^-$ to TN was evaluated using the GFP-Atg18 marker as described above. Unexpectedly, the percentage of cells that contained GFP-Atg18 puncta after a TN treatment was higher in the *ireA*$^-$ strain than in the WT strain (Fig. 7A and B). This increase is evident in the number of cells with three or more GFP-Atg18 puncta, which is even higher than that observed under starvation conditions in both strains. However, TN-induced GFP-Atg18 puncta in *ireA*$^-$ cells appeared larger compared to the tiny puncta observed in WT cells after the same treatment or even in *ireA*$^-$ cells under starvation conditions (Fig. 7A). Large puncta may result from the accumulation of abnormal autophagosomes unable to degrade their cargo, as observed previously in the *Dictyostelium* autophagic *vmp1*$^-$ mutant (60). To clarify this possibility, the *ireA*$^-$ mutant was exposed to TN, and the autophagy flux was evaluated using the GFP-PgkA proteolytic assay described above (Fig. 7C and D). Under these conditions, the level of free GFP accumulated in the *ireA*$^-$ cells was significantly lower than in the WT cells. In contrast, the level of free GFP in the absence of stress did not differ significantly between WT and *ireA*$^-$ strains, indicating that the autophagy degradation defect of *ireA*$^-$ cells occurs specifically under ER stress conditions. Similar experiments were performed in *ireA*$^-$ cells expressing the K603N or N927A mutant forms to determine the requirement of the kinase and KEN domains in the TN-induced autophagic response (Fig. 8A and B). Compared to the WT strain, *ireA*$^-$ mutant strains presented a significantly reduced amount of accumulated free-GFP, indicating that both IreA domains are required for productive TN-induced autophagy. Immunoblot detection of the IreA mutant forms was performed with an anti-GFP antibody to evaluate whether the IreA forms were degraded after the consecutive TN and NH_4Cl treatments. As can be observed in overexposed membrane (Fig. 8C), under this treatment free GFP was not significantly generated by these constructs compared to cells expressing the GFP-PgkA construct, and therefore the detected free GFP reflects only the autophagic degradation of the cytosolic GFP-PgkA.

It has been reported that *Dictyostelium* autophagy-deficient cells accumulate ubiquitin-positive aggregates and that the ineffective degradation of these protein aggregates can be used as a reliable marker of autophagy inhibition (61, 62). These ubiquitin-positive protein aggregates can be visualized by confocal microscopy using immunofluorescence techniques (62). As shown in Fig. 9, *ireA*$^-$ cells expressing the autophagic marker GFP-Atg18 exhibited large ubiquitin-positive aggregates after a TN treatment; such aggregates were absent in WT cells, further supporting that the autophagy flux after TN treatment is impaired in the absence of IreA. Interestingly, some the ubiquitin-containing aggregates are closed to enlarged GFP-Atg18 puncta. Together, all these results suggest that under ER stress, *ireA*$^-$ cells are unable to degrade autophagic cargoes, even though autophagy induction is not altered.

***ireA*$^-$ cells present abnormal autophagic structures and a collapsed endoplasmic reticulum after ER stress.** It has been observed that during autophagy induction, Atg18 (WIPI-1) localizes transiently at autophagosome initiation sites in *Dictyostelium* and human cells (27, 63). Mutant cells with defective autophagosome closure present abnormal Atg18 recruitment patterns (60, 64). The autophagosome assembly can be followed by detection of GFP-tagged Atg18 with live time-lapse confocal microscopy. WT and *ireA*$^-$ cells expressing this marker were treated with TN for 7 h, and then the cells were monitored for 900 s (Fig. 10A; see also Movies S1 and S2 in the supplemental material). A specific GFP-Atg18 puncta was selected and followed on the *z*-axis until it was no longer visible. In WT cells, GFP-Atg18 could only be visualized for short periods of time ranging from 30 to 80 s, as previously described (27). In contrast, the GFP-Atg18-positive elongated structures in *ireA*$^-$ cells were very static and persisted during the entire time course of this experiment (900 s). These data, together with the

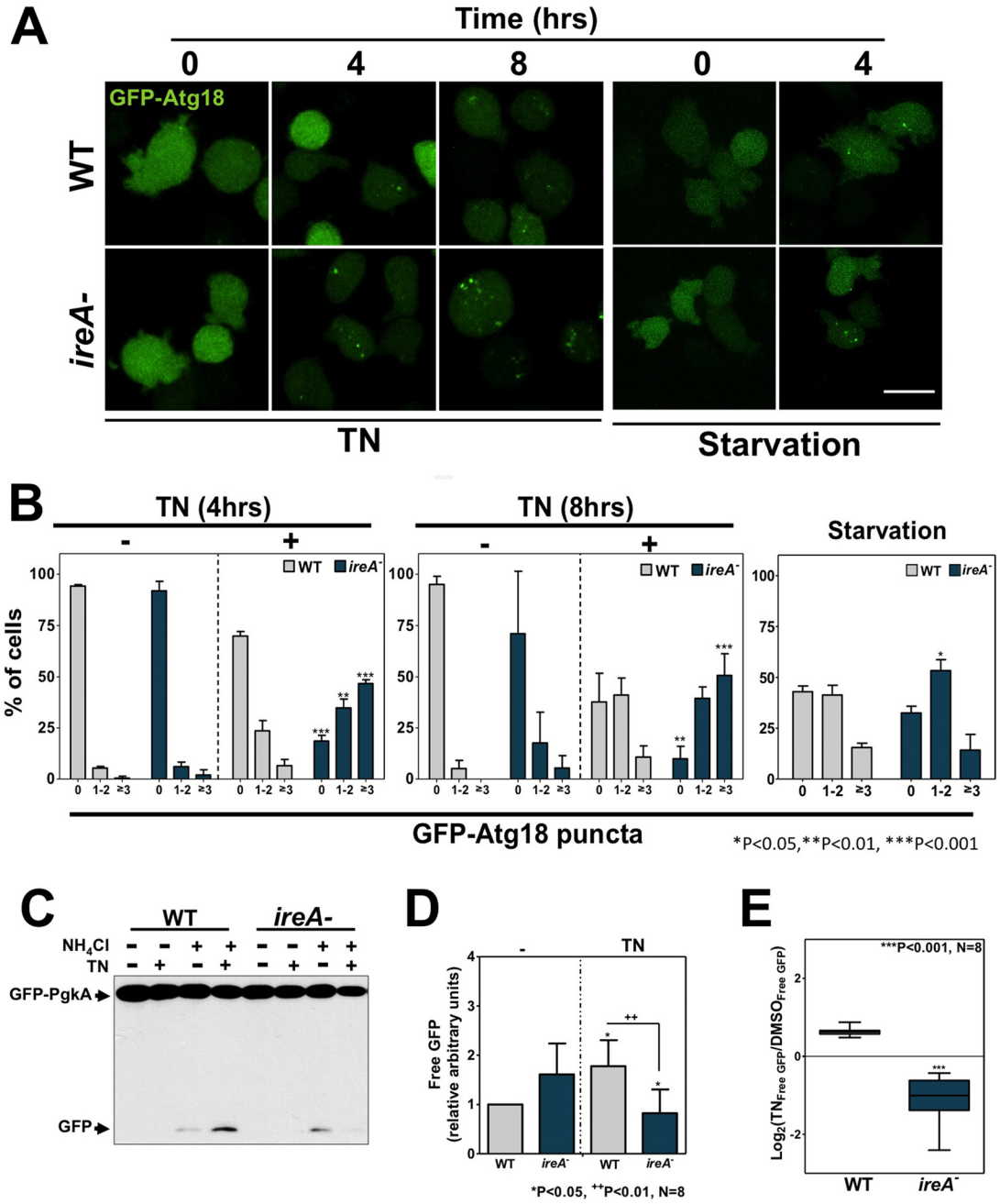

FIG 7 The absence of IreA alters ER stress-induced autophagy. (A) Autophagy was determined as punctum formation in cells expressing GFP-Atg18 (maximum intensity z-projection representative picture). WT and *ireA*$^-$ cells were treated with 2 μg/ml TN or incubated in starvation buffer for the indicated times. Cells were visualized *in vivo* by confocal microscopy (scale bar, 10 μm). (B) Percentages of cells containing 0, 1 or 2, or ≥3 GFP-Atg18 puncta. Values are means ± the SD of three independent experiments. Asterisks denote statistically significant differences. (C) Representative Western blot of a NH_4Cl-induced GFP-PgkA cleavage assay. WT and *ireA*$^-$ cells overexpressing the GFP-PgkA were treated for 8 h with 2 μg/ml TN. During the last 2 h of treatment, cells were incubated in the presence or absence of NH_4Cl as described in Materials and Methods. (D) Quantification of accumulated free GFP in WT and *ireA*$^-$ cells determined by densitometry. Mean values ± the SD of eight independent experiments were graphed. GFP was normalized against GFP-PgkA and refers to untreated cells. Asterisks indicate statistically significant differences. (E) Means ± the SD of the $\log_2$ ($TN_{free\ GFP}/DMSO_{free\ GFP}$) from the data in panel D.

observations of the decreased degradation capacity of *ireA*$^-$ cells upon a TN treatment, suggest that the lack of IreA impairs the regulation of autophagosome assembly.

It has been reported that ER stress causes expansion of the ER membrane (21), and our expression data suggest that after TN treatment the ER membrane composition may be adapted to cope with ER stress in *Dictyostelium* cells. In addition, we observed

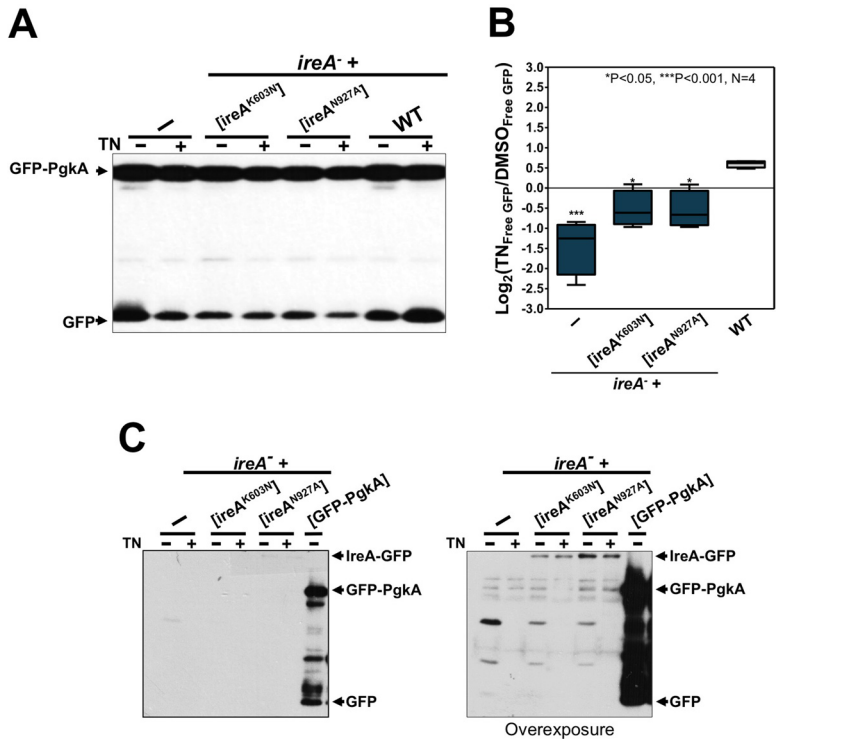

FIG 8 Expression of inactive IreA forms cannot rescue autophagy blockage caused by IreA disruption. (A) NH_4Cl-induced GFP-PgkA cleavage assay. A representative Western blot is shown. WT and *ireA*$^-$ cells expressing the indicated constructs were not treated or treated for 8 h with 2 μg/ml TN. During the last 2 h of treatment, cells were incubated in the presence of NH_4Cl as described in Materials and Methods. (B) Means $\pm$ the SD of the $\log_2(TN_{free\ GFP}/DMSO_{free\ GFP})$ derived from densitometries of the gel in panel A. Free GFP accumulation was normalized against GFP-PgkA and referred to GFP accumulation in the WT strain treated with vehicle alone (DMSO). Values represent the mean of four independent experiments. Significant differences are indicated by asterisks. (C) *ireA*$^-$ cells expressing the GFP-tagged K603N or N927A IreA constructs were treated with DMSO or TN and incubated with NH_4Cl.

that ER morphology maintenance upon ER stress depends on a fully functional IreA. Considering that the ER membrane serves as a platform for autophagosome formation in *Dictyostelium* and mammalian cells (27, 61, 65), we hypothesized that the aberrant autophagic structures in *ireA*$^-$ cells may arise from ER dysfunction. To address this possibility, we analyzed ER morphology by immunodetection of PDI in cells expressing the GFP-Atg18 protein. We found that IreA-deficient cells under TN treatment lost the normal structure and distribution of the ER cisternae, which appeared collapsed in large perinuclear structures (Fig. 10B; see also Movie S3 in the supplemental material). In contrast to the WT strain, the aberrant ER of the *ireA*$^-$ mutant presented conspicuous and elongated GFP-Atg18 structures (Fig. 10B and C). These observations support the idea that autophagosome assembly at the ER is impaired in the *ireA*$^-$ cells as a consequence of its inability to restore ER homeostasis upon TN treatment.

DISCUSSION

In this work we present the first characterization of the *Dictyostelium* ER stress response and the UPR pathway. We identified IreA as an essential UPR regulator and studied its connection and relationship with autophagy. *Dictyostelium* contains a single IreA gene, which facilitates the analysis of the role of this sensor in comparison to other organisms such as humans (66) or *A. thaliana* (12), which contain two orthologues. Furthermore, the ER in *Dictyostelium* seems to present more structural similarities with high-order eukaryotes than with yeasts, as can be inferred from microscopy observations from this and other reports (67, 68), making it a good model system for ER-related processes.

Our genome-wide expression data analysis shows that *Dictyostelium* UPR regulates

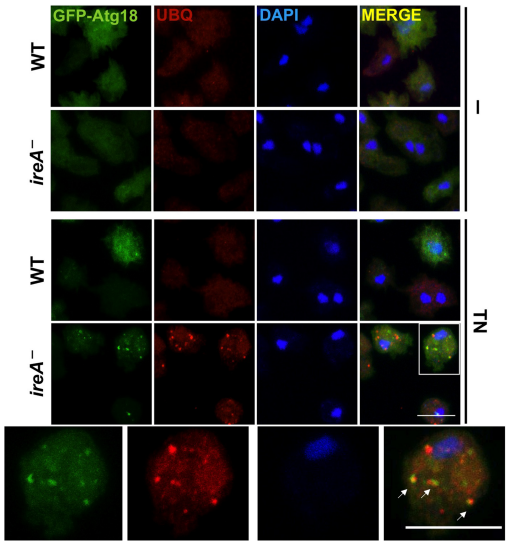

FIG 9 *ireA*$^-$ cells accumulate aberrant ubiquitin aggregates after TN treatment. Confocal microscopy images of WT and *ireA*$^-$ cells expressing GFP-Atg18 are shown. Cells were fixed and labeled for immunofluorescence detection with an anti-human ubiquitin antibody (red) after 8 h treatment with 2 μg/ml TN or vehicle alone. Nuclei were stained with DAPI. Arrows indicate GFP-Atg18 and ubiquitin colocalization. Scale bars, 10 μm.

the levels of specific mRNAs upon ER stress, and we concluded that, as described in yeast and mammalian cells (7, 69), *Dictyostelium* adapts to ER stress conditions by increasing the expression of proteins involved in protein folding and degradation processes. Also, a decrease in the ER protein load is achieved by downregulating the expression of genes that are targeted to membranes and to the secretory pathway, among others. Both parts of this transcriptional reprogramming partially depend on IreA, which may activate a transcriptional factor, as described in other organisms (66), since its RNase activity results essential for cell survival and for proper IreA-clustering kinetics after a TN treatment. However, bioinformatics analyses failed to identify an orthologue of the bZIP HAC1/XBP1 transcription factor encoded by the *Dictyostelium* genome. This does not rule out the possible existence of such protein in *Dictyostelium*, since these transcription factors show scarce amino acid similarities between species (70).

In *Schizosaccharomyces pombe* and *Candida glabrata* no homologues of a canonical HAC1/XBP1 have been identified, and the Ire1 RNase activity has been shown to be involved in the degradation of mRNAs in a process known as regulated Ire1-dependent decay of mRNA (RIDD) (52, 71). This process is also part of the UPR in other organisms, such as *Drosophila* and humans (4), and in *Dictyostelium* a similar mechanism could be responsible for the IreA-dependent downregulation of some mRNAs after TN treatment. In addition, the fact that *S. pombe* Ire1 can increase the BiP-mRNA stability directly by processing its 3′ untranslated region (52) opens new possibilities for a direct role of Ire1 in the positive regulation of mRNA stability. This function of Ire1 could be conserved in other organisms in which a canonical HAC1/XBP1 homologue has not been identified, such as *Dictyostelium*.

Almost half of the transcriptional response to the TN treatment in *Dictyostelium* cells is independent of IreA, thus supporting the existence of other ER stress transducers. In animal and plant cells, the UPR is mediated, in addition to Ire1, by ATF6 homologues (72). These ER-resident transmembrane bZIP transcription factors are liberated from the ER under ER stress conditions and translocate to the nucleus to contribute to the transcriptional activation of protein-folding-associated genes, such as the Grp78 gene (72, 73), although we could not identify by BLAST analysis any ATF6 orthologue gene in the *Dictyostelium* genome. In animal cells, ER stress-induced transcriptional regula-

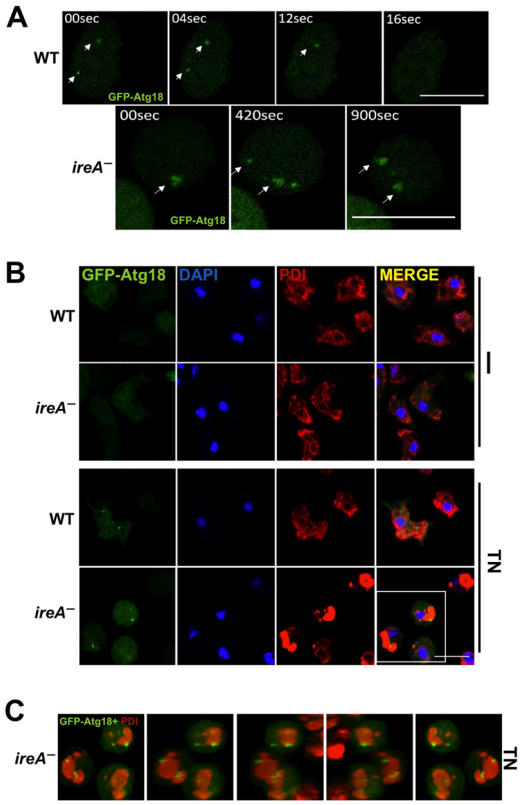

FIG 10 *ireA*⁻ cells exhibit long-lived GFP-Atg18 aberrant structures upon ER stress. (A) Time-lapse confocal images of WT and *ireA*⁻ cells expressing GFP-Atg18 after a 7-h treatment with 2 μg/ml TN. Arrows indicate the same GFP-Atg18 structure in the different time exposures. The corresponding video lapses are included as Movies S1 and S2 in the supplemental material. (B) Confocal microscopy images of WT and *ireA*⁻ cells expressing GFP-Atg18 and prepared for immunodetection of the ER marker PDI (red). Cells were treated for 8 h with 2 μg/ml TN or with vehicle alone. Nuclei were stained with DAPI. (C) Rotational views of a three-dimensional (3D) reconstruction of *ireA*⁻ TN-treated cells. A complete 3D reconstruction is provided in Movie S3 in the supplemental material. Scale bars (A and B), 10 μm.

tion is mediated also by the ER membrane-resident eukaryotic translation initiation factor 2α (eIF2α) kinase PERK; nevertheless, orthologues of this protein have not been identified in fungi or plants (74). BLAST analysis identifies two eIF2α kinases encoded by the *Dictyostelium* genome. However, these proteins have been described as functionally related to yeast Gcn2p, another eIF2α kinase involved in amino acid metabolism (45, 75).

The assembly of Ire oligomers correlates with Ire1 activation and persists only until the adaptation state is reached (50, 76). From our data on oligomer formation it can be inferred that IreA may get activated after a short time of TN treatment (2 h), and adaption under persistent ER stress might take place after longer periods (8 h). In yeast, it has been observed that inactivation of both Ire1 kinase and RNase domains cause persistent Ire1 clustering upon ER stress, indicating that Ire1 activity is required to regulate its activation-inactivation switch during the adaptation process (77). Consistently, IreA must be fully active to properly regulate its clustering behavior during sustained ER stress in *Dictyostelium*.

It has been widely described that ER stress-inducing treatments trigger autophagy. Our data support these observations and, together with the reports from yeasts (21, 33), mammals (30, 78), insects (79, 80), and plants (32, 34), show that this process is highly conserved between species. Despite the TN-induced autophagy in *Dictyostelium* and the sensitivity of autophagy-defective mutants to ER stress, we did not detect any change in the expression of *atg* genes in our whole-genome expression analysis. Since *Dictyostelium* cells possess a highly active autophagy machinery during vegetative

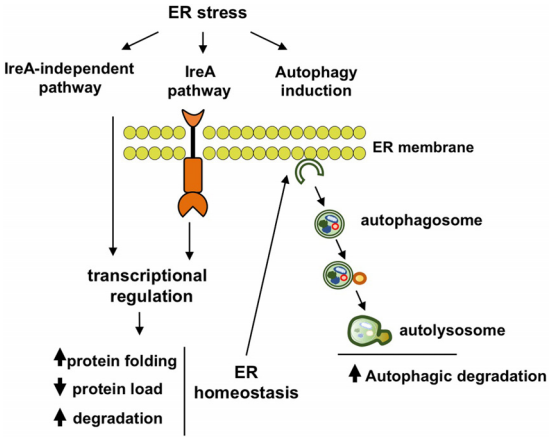

FIG 11 Graphical model of the *Dictyostelium* response to ER stress. IreA and other unknown sensors detect the ER stress stimulus. In turn, they restore ER stability by triggering a transcriptional response that increases the protein folding and degradation capacity of the cell while decreasing the protein load at the ER. Autophagy is also induced in an IreA-independent manner as a response to ER stress and contributes to increase the cellular degradation capacity of cells. ER homeostasis recovery by IreA-dependent and -independent pathways is essential in order to achieve a functional increase in autophagy-associated degradation.

growth (62), an increase in the expression of these genes may not be required. However, we found that the transcript levels of the gene encoding sqstm1 (p62) (61), a protein involved in the degradation of ubiquitinated protein aggregates by autophagy (81), are highly induced. This, together with the observation that the expression of the ERAD retrotranslocation protein CdcD (VCP/p96 orthologue) is also highly induced, suggest that autophagy in *Dictyostelium* may in part participate in the degradation of cytosolic ubiquitinated aggregates that arise from protein retrotranslocation. Autophagy might also be clearing ER-derived nonfunctional membranes, a recovery mechanism that has been observed in stressed yeast (21).

This is the first work evaluating the induction of autophagy upon ER stress in an organism with a complete depletion of Ire1 activity. The autophagy phenotype of single knockouts of both Ire1 plant homologues was analyzed in a previous report (28), and similar analyses were performed in mammalian cells using small interference RNAs (30), a technique that might not completely deplete the expression of the target protein. Yorimitsu et al. (31) reported that in yeasts Ire1-depleted cells under ER stress may show an autophagy blockage, but no experimental data were presented. We observed that autophagy is induced in IreA-depleted cells after a TN treatment, since there is an increase in GFP-Atg18 puncta. However, these structures are persistent, abnormal, and trapped at the ER after TN treatment. In addition, the accumulation of ubiquitinated aggregates and the reduced degradation of GFP-PgkA observed in the *ireA*$^{-}$ strain strongly suggest that these GFP-Atg18-positive structures are unable to degrade cargoes during ER stress. This characteristic is similar to that observed in VMP1-depleted cells in *Dictyostelium* (61). VMP1 is an ER-resident protein involved in the maintenance of ER structure, autophagy, and the regulation of membrane contact sites between the ER and other organelles (68, 82). These phenotypic similarities suggest that abnormalities in the ER might impair the formation of functional omegasomes, the ER-derived structures required for autophagosome formation (83), thereby leading to a blockage in autophagy-dependent degradation.

Our data support a model in which ER stress activates IreA-dependent and -independent pathways (Fig. 11). These pathways cooperate to restore ER homeostasis by reducing the ER protein load and by increasing the protein folding and degradation capacities of the cell. Autophagy is also induced after ER stress in an IreA-independent manner, but complete autophagosome assembly can only proceed if ER homeostasis and the ER structure have been restored. Our findings highlight the delicate balance between

autophagy and ER homeostasis and pinpoint IreA as an important component of this functional relationship.

MATERIALS AND METHODS

***Dictyostelium* cell growth, transformation, and development.** All of the strains used in this study were derived from *D. discoideum* strain AX4. Cells were grown at 22°C in a standard microbiology incubator. Axenic growth was performed in HL5 medium (Formedium, catalog no. HLB0102) supplemented with 1% glucose and penicillin-streptomycin (10,000 U/ml penicillin and 10,000 mg/ml streptomycin; Gibco). For growth in association with bacteria, *K. aerogenes* (Ka strain) was spread onto SM agar plates (1% glucose [Sigma], 1% peptone [Difco], 0.1% yeast extract, 4 mM $MgSO_4$, 13 mM KH_2PO_4, 3 mM K_2HPO_4, and 2% agar). Starvation was induced in PDF buffer (20 mM KCl, 9 mM K_2HPO_4, 13 mM KH_2PO_4, 1 mM $CaCl_2$, 1 mM $MgSO_4$ [pH 6.4]). For drug treatments, stock solutions were prepared, and working solutions at the desired concentrations were prepared by diluting fresh stock aliquots each time in HL5 at the indicated concentrations. Tunicamycin (Enzo Life Sciences) was prepared in DMSO. DTT (Thermo Fisher Scientific) and 2-DOG (Sigma) were diluted in water. All treatments were performed on axenically growing cells at exponential phase.

For transformation, 5×10^6 cells were washed with H50 buffer (4.76 g/liter HEPES, 3.73 g/liter KCl, 0.58 g/liter NaCl, 0.12 g/liter $MgSO_4$, 0.42 g/liter $NaHCO_3$, 0.156 g/liter NaH_2PO_4 [pH 7]) and electroporated with 2 to 10 μg of linear or plasmid DNA. The detailed procedure and the antibiotic concentrations used for selection are described elsewhere (84).

The *ireA* mutant strain was generated by homologous recombination. Cells were transformed with a 2,773-bp PCR product obtained from the pGEM-[*ireA*::*BST*] construct (see "Plasmid constructs" below). After selection with blasticidin, the transformants were plated on SM plates with *K. aerogenes* for clonal isolation. Homologous recombination was evaluated by colony PCR. For this, DNA was extracted with Master Amp DNA extraction solution (Epicentre) and tested with the indicated oligonucleotides (see Fig. 2 and Results). Other strains used in this study (*atg1*$^-$, *atg13*$^-$, and *atg101*$^-$ strains) have been described previously (59). For the development assays 5×10^7 cells growing axenically in HL5 were collected, centrifuged at 1,000 rpm for 5 min, washed two times, and then resuspended in PDF buffer before depositing them in nitrocellulose filters (Millipore, catalog no. HABP04700) soaked in PDF buffer.

Serial dilution spot assays. Exponentially growing cells were adjusted at 10^6 cells/ml density and then subjected to the indicated treatments at the specified concentrations and times. After the treatment, 10-fold serial dilutions were prepared, and 4 μl of each dilution was spotted over a lawn of *K. aerogenes* previously plated on SM agar plates. Depending on the experiment, pictures were taken after 5 to 7 days of incubation at 22°C. All spot assays were performed at least three times.

Plasmid constructs. The *ireA* gene was amplified from genomic DNA, cloned into the pGEM-T Easy vector (Promega), and used as the template for all other constructs. All the IreA-GFP fusion constructs were expressed in *Dictyostelium* using the extrachromosomal pDM323 plasmid (85). PCR products were inserted between the BglII and SpeI sites of this plasmid. Point mutations were introduced by PCR using as the template the complete pGEM-T-[*ireA*] plasmid according to a previously described protocol (86). All constructs were completely sequenced. The pBluescript II containing the blasticidin resistance cassette cloned between EcoRI and HindIII (pBSII-[BST]) (87), was used to generate the *ireA*::*BST* construction. To generate the pGEM-T-Easy-[*ireA*::*BST*] construct, the SmaI/KpnI fragment of pBSII-[BST] was introduced between the EcoRV and KpnI sites of the pGEM-T-Easy-[*ireA*] vector. Then, to generate the *ireA*::*BST* knockout strain, the construct was amplified by PCR with *ireA*-specific oligonucleotides, and *Dictyostelium* AX4 WT cells were electroporated with 5 μg of purified PCR product (see above). Insertion of the BST cassette interrupted the *ireA* gene and caused a 998-bp deletion in the locus (see Fig. 2 and Results). pSJSK489 plasmid expressing GFP-Atg18 was kindly provided by J. King. pDM358 expressing the PgkA-GFP fusion was generated as described previously (56).

RNA extraction and deep RNA sequencing. Cells were adjusted to a density of 10^6 cells/ml and treated for 16 h with 2 μg/ml TN or DMSO in HL5. Cells were separated by centrifugation from this medium and washed with PDF buffer. RNA was extracted according to a standard TRIzol protocol (Sigma). cDNA libraries were prepared from total RNA using a TruSeq sample preparation v2 kit (Illumina), according to the manufacturer's recommendations. Briefly, poly(A) containing mRNA was purified from 1 μg using poly(T) oligonucleotide-attached magnetic beads [oligo(dT) magnetic beads]. Once purified, the mRNA was fragmented using divalent cations under high temperature. After fragmentation, first-strand cDNA was synthesized using reverse transcriptase and random primers, and then a second strand was generated using DNA polymerase I and RNase H. cDNA fragments were end repaired, and a single "A" base was added (to the 3′ end of the blunt fragment); barcoded (indexed) adapters were then ligated to each sample. The products were purified and enriched with a 15-cycle PCR to obtain the final cDNA libraries.

Libraries were validated using an Agilent tape station system. Samples were normalized and pooled for sequencing on an Illumina MiSeq. Libraries at a 9 pM concentration were run using a 150-bp single-read protocol. An RNA deep sequencing (RNA-seq) experiment was performed with two biological replicates. This assay was performed at the sequencing service of the molecular biology facility of the Instituto de Fisiología Celular (IFC), UNAM, Mexico.

RNA-seq data assembly was performed using TopHat and Cufflinks (88), and the set of significantly differentially expressed genes was obtained using the two biological replicates (raw data can be found at NCBI GEO database under accession number GSE104409). The obtained list was further filtered in order to contain only genes that were represented by ~1 mRNA per cell in one of the two compared conditions. In accordance to Parikh et al. (89), using our conditions 1 mRNA would be represented by 15

normalized read counts. The genes that presented a $\log_2$ fold change of ≥ 1.3 or ≤ -1.3 between the tested conditions (see Archive S1 in the supplemental material) were further analyzed and classified in enriched gene ontology categories with the DAVID functional annotation tool (53, 54), using the biological process (GOTERM_BP_DIRECT), cellular component (GOTERM_CC_DIRECT), and protein domains (INTERPRO) categories, with default settings.

Bioinformatic analysis. *Dictyostelium* sequences were obtained from the dictyBase (90), and BLAST searches were also performed using the tool provided in this database. Protein sequences from other organisms were obtained from the UniProt database (91). The SIM alignment tool (92) was used for local protein alignments, and results were visualized with LALNVIEW (93). Multiple alignments were performed with CLUSTAL OMEGA (57). The assembly of the data obtained from the deep RNA sequencing of poly(A) RNA was performed using the TopHat and Cufflinks open source software as described previously (88). Ontology enrichment analyses were performed with the PANTHER (94) and DAVID (53, 54) web tools.

Microscopy. Exponentially growing cells were adjusted to 10^6 cells/ml, treated as specified, and transferred to Ibidi m-Slide 8-well slides. The cells were then directly observed *in vivo* (for cells expressing fluorescently tagged proteins) or fixed for immunofluorescence detection. For this procedure, cells were fixed for 15 min after the desired treatment with 2% paraformaldehyde dissolved in phosphate-buffered saline or PDF buffer. Primary antibody incubation was performed overnight at 4°C. Antibody to *Dictyostelium* PDI was kindly provided by Pierre Cosson, and anti-human ubiquitin (P4D1) 3936 was purchased from Cell Signaling (used at 1:1,000 and 1:500 dilutions, respectively). For fluorescence detection, preparations were incubated 30 min at room temperature with a secondary antibody conjugated to Alexa Fluor red 546. Nuclei were stained with DAPI (4′,6′-diamidino-2-phenylindole). Confocal images were acquired with an inverted Zeiss spectral LSM710 microscope. To evaluate cell morphology, cells were deposited on standard microscope slides and analyzed with an inverted phase-contrast microscope. Cells developing in nitrocellulose filters were visualized with a Nikon SMZ800 microscope.

Western blotting. After the specified treatments, the cells were washed with PDF buffer and resuspended in lysis buffer (10 mM Tris-HCl [pH 7.5], 150 mM NaCl, 0.5 mM EDTA, 0.5% NP-40, 0.05% SDS) supplemented with a fresh protease inhibitor cocktail (Sigma), followed by incubation for 30 min on ice. The total protein concentration was assayed from cleared protein extracts using a BCA commercial kit (Thermo Fisher Scientific). Total cell extracts were subjected to SDS-PAGE separation and transferred to polyvinylidene difluoride membranes (Millipore). Immunoblot detection was performed with the following specified antibodies: anti-GFP (Sigma-Aldrich, G1544), anti-Grp78 (Santa Cruz Biotechnology, sc-1050, goat anti-human GRP78 [N-20], discontinued), or anti-cdcD (Vcp/P97; rabbit anti-*Dictyostelium* CdcD, kindly provided by Ludwig Eichinger [43]). MCCC1 was used as an internal load control and was detected by using streptavidin conjugated to horseradish peroxidase as described elsewhere (95). Densitometric analysis of Western blot images was performed with ImageJ software. These measurements were used to determine arbitrary protein level values. MCCC1 or GFP-PgkA was used for normalization.

Autophagy assays. Cells expressing GFP-Atg18 were analyzed by live confocal microscopy imaging, and punctum-containing cells were quantified manually with ImageJ software by analyzing maximum z-projections and comparing them with individual stacks.

Autophagy capacity was evaluated using a modification of the previously described proteolytic assay (56, 58). PgkA-GFP-expressing cells were adjusted to 10^6 cells/ml and then treated for 8 h with 2 μg/ml TN or vehicle (DMSO). During the last 2 h of treatment, two 1-h pulses of 150 mM NH_4Cl were applied. The cells were then collected, lysed, and prepared for Western blot analysis as described above. The accumulation of free GFP was quantified by densitometry and normalized against GFP-PgkA.

Statistical analyses. Mean values, standard deviations (SD), and significance were graphed and analyzed from at least three independent experiments using GraphPad Prism 5. Statistical significance was tested with either a Student *t* test, a one-way analysis of variance (ANOVA) with Dunnett's posttest, or a two-way ANOVA with a Bonferroni posttest depending on the number of variables for the experiment.

Accession number(s). The raw RNA-seq data analyzed during the present study are available from the NCBI GEO database under accession number GSE104409.

SUPPLEMENTAL MATERIAL

Supplemental material for this article may be found at https://doi.org/10.1128/MCB.00054-18.

SUPPLEMENTAL FILE 1, AVI file, 1.4 MB.
SUPPLEMENTAL FILE 2, AVI file, 2.4 MB.
SUPPLEMENTAL FILE 3, AVI file, 1.6 MB.
SUPPLEMENTAL FILE 4, XLS file, 0.2 MB.
SUPPLEMENTAL FILE 5, XLS file, 0.1 MB.
SUPPLEMENTAL FILE 6, XLS file, 0.1 MB.
SUPPLEMENTAL FILE 7, XLS file, 0.1 MB.
SUPPLEMENTAL FILE 8, XLS file, 0.1 MB.
SUPPLEMENTAL FILE 9, XLS file, 0.1 MB.

ACKNOWLEDGMENTS

We acknowledge the technical assistance of the staff at the Unidad de Cómputo and Unidad de Biología Molecular, IFC, Universidad Nacional Autónoma de México (UNAM), and the microscopy facility at Instituto de Investigaciones Biomédicas Alberto Sols. We particularly thank Diego Navarro Vera for his assistance.

E.D.-M. is a Ph.D. student from Programa de Doctorado en Ciencias Biomédicas, Universidad Nacional Autónoma de México (UNAM), and the Programa de Doctorado en Biociencias Moleculares, Universidad Autónoma de Madrid (UAM), supported by CONACyT (380127) (261212), PAEP, and Banco Santander (Catedra Isaac Costero). This study was supported by grants BFU2012-32536 and BFU2015-64440-P from the Ministerio de Economía, Industria y Competitividad and by FEDER (E.D.-M., O.V., and R.E.) and by grants from CONACyT (CB-254078) and PAPIIT, DAGAPA, UNAM (IN210616) to R.C.

REFERENCES

1. Snapp E. 2005. Endoplasmic reticulum biogenesis: proliferation and differentiation, p 63–95. Landes Bioscience/Kluwer Academic/Plenum Publishers, New York, NY.
2. Fagone P, Jackowski S. 2009. Membrane phospholipid synthesis and endoplasmic reticulum function. J Lipid Res 50(Suppl):S311–S316. https://doi.org/10.1194/jlr.R800049-JLR200.
3. Scheuner D, Song B, McEwen E, Liu C, Laybutt R, Gillespie P, Saunders T, Bonner-Weir S, Kaufman RJ. 2001. Translational control is required for the unfolded protein response and *in vivo* glucose homeostasis. Mol Cell 7:1165–1176. https://doi.org/10.1016/S1097-2765(01)00265-9.
4. Maurel M, Chevet E, Tavernier J, Gerlo S. 2014. Getting RIDD of RNA: IRE1 in cell fate regulation. Trends Biochem Sci 39:245–254. https://doi.org/10.1016/j.tibs.2014.02.008.
5. Lee A, Iwakoshi N, Glimcher L. 2003. XBP-1 regulates a subset of endoplasmic reticulum resident chaperone genes in the unfolded protein response. Mol Cell Biol 23:7448–7459. https://doi.org/10.1128/MCB.23.21.7448-7459.2003.
6. Sriburi R, Jackowski S, Mori K, Brewer JW. 2004. XBP1: a link between the unfolded protein response, lipid biosynthesis, and biogenesis of the endoplasmic reticulum. J Cell Biol 167:35–41. https://doi.org/10.1083/jcb.200406136.
7. Travers KJ, Patil CK, Wodicka L, Lockhart DJ, Weissman JS, Walter P. 2000. Functional and genomic analyses reveal an essential coordination between the unfolded protein response and ER-associated degradation. Cell 101:249–258. https://doi.org/10.1016/S0092-8674(00)80835-1.
8. Ron D, Walter P. 2007. Signal integration in the endoplasmic reticulum unfolded protein response. Nat Rev Cell Biol 8:519–529. https://doi.org/10.1038/nrm2199.
9. Chen Y, Brandizzi F. 2013. IRE1: ER stress sensor and cell fate executor. Trends Cell Biol 23:547–555. https://doi.org/10.1016/j.tcb.2013.06.005.
10. Gardner BM, Walter P. 2011. Unfolded proteins are Ire1-activating ligands that directly induce the unfolded protein response. Science 333:1891–1894. https://doi.org/10.1126/science.1209126.
11. Kimata Y, Kimata YI, Shimizu Y, Abe H, Farcasanu IC, Takeuchi M. 2003. Genetic evidence for a role of BiP/Kar2 that regulates Ire1 in response to accumulation of unfolded proteins. Mol Biol Cell 14:2559–2569.
12. Nagashima Y, Mishiba K, Suzuki E, Shimada Y, Iwata Y, Koizumi N. 2011. *Arabidopsis* IRE1 catalyses unconventional splicing of bZIP60 mRNA to produce the active transcription factor. Sci Rep 1: 29. https://doi.org/10.1038/srep00029.
13. Kawahara T, Yanagi H, Yura T, Mori K. 1997. Endoplasmic reticulum stress-induced mRNA splicing permits synthesis of transcription factor Hac1p/Ern4p that activates the unfolded protein response. Mol Biol Cell 8:1845–1862. https://doi.org/10.1091/mbc.8.10.1845.
14. Bowring C, Llewellyn D. Differences in HAC1 mRNA processing and translation between yeast and mammalian cells indicate divergence of the eukaryotic ER stress response. Biochem Biophys Res Commun 287:789–800.
15. Iwata Y, Koizumi N. 2005. An *Arabidopsis* transcription factor, AtbZIP60, regulates the endoplasmic reticulum stress response in a manner unique to plants. Proc Natl Acad Sci U S A 102:5280–5285. https://doi.org/10.1073/pnas.0408941102.
16. Cox JS, Walter P. 1996. A novel mechanism for regulating activity of a transcription factor that controls the unfolded protein response. Cell 87:391–404. https://doi.org/10.1016/S0092-8674(00)81360-4.
17. Martinez IM, Chrispeels MJ. 2003. Genomic analysis of the unfolded protein response in *Arabidopsis* shows its connection to important cellular processes. Plant Cell 15:561–576. https://doi.org/10.1105/tpc.007609.
18. Ruggiano A, Foresti O, Carvalho P. 2014. Quality control: ER-associated degradation: protein quality control and beyond. J Cell Biol 204:869–879. https://doi.org/10.1083/jcb.201312042.
19. Tsai B, Ye Y, Rapoport Ta. 2002. Retro-translocation of proteins from the endoplasmic reticulum into the cytosol. Nat Rev Mol Cell Biol 3:246–255. https://doi.org/10.1038/nrm780.
20. Yorimitsu T, Klionsky DJ. 2007. Eating the endoplasmic reticulum: quality control by autophagy. Trends Cell Biol 17:279–285. https://doi.org/10.1016/j.tcb.2007.04.005.
21. Bernales S, McDonald KL, Walter P. 2006. Autophagy counterbalances endoplasmic reticulum expansion during the unfolded protein response. PLoS Biol 4:e423. https://doi.org/10.1371/journal.pbio.0040423.
22. Cheng Y. 2011. Survival and death of endoplasmic-reticulum-stressed cells: role of autophagy. World J Biol Chem 2:226–231. https://doi.org/10.4331/wjbc.v2.i10.226.
23. Klionsky DJ, Emr SD. 2000. Autophagy as a regulated pathway of cellular degradation. Science 290:1717–1721. https://doi.org/10.1126/science.290.5497.1717.
24. Kroemer G, Mariño G, Levine B. 2010. Autophagy and the integrated stress response. Mol Cell 40:280–293. https://doi.org/10.1016/j.molcel.2010.09.023.
25. Russell RC, Yuan H-X, Guan K-L. 2014. Autophagy regulation by nutrient signaling. Cell Res 24:42–57. https://doi.org/10.1038/cr.2013.166.
26. Filomeni G, Zio DD, Cecconi F, De Zio D, Cecconi F. 2015. Oxidative stress and autophagy: the clash between damage and metabolic needs. Cell Death Differ 22:377–388. https://doi.org/10.1038/cdd.2014.150.
27. King JS, Veltman DM, Insall RH. 2011. The induction of autophagy by mechanical stress. Autophagy 7:1490–1499. https://doi.org/10.4161/auto.7.12.17924.
28. Desai M, Fang R, Sun J. 2015. The role of autophagy in microbial infection and immunity. Immunotargets Ther 4:13–27. https://doi.org/10.2147/ITT.S76720.
29. Suh DH, Kim M-K, Kim HS, Chung HH. 2012. Unfolded protein response to autophagy as a promising druggable target for anticancer therapy. Ann N Y Acad Sci 1271:20–32. https://doi.org/10.1111/j.1749-6632.2012.06739.x.
30. Ogata M, Hino S-I, Saito A, Morikawa K, Kondo S, Kanemoto S, Murakami T, Taniguchi M, Tanii I, Yoshinaga K, Shiosaka S, Hammarback Ja Urano F, Imaizumi K. 2006. Autophagy is activated for cell survival after endoplasmic reticulum stress. Mol Cell Biol 26:9220–9231. https://doi.org/10.1128/MCB.01453-06.
31. Deegan S, Koryga I, Glynn SA, Gupta S, Gorman AM, Samali A. 2014. A close connection between the PERK and IRE arms of the UPR and the transcriptional regulation of autophagy. Biochem Biophys Res Commun 456:305–311. https://doi.org/10.1016/j.bbrc.2014.11.076.

32. Liu Y, Burgos JS, Deng Y, Srivastava R, Howell SH, Bassham DC. 2012. Degradation of the endoplasmic reticulum by autophagy during endoplasmic reticulum stress in *Arabidopsis*. Plant Cell 24:4635–4651. https://doi.org/10.1105/tpc.112.101535.
33. Yorimitsu T, Nair U, Yang Z, Klionsky DJ. 2006. Endoplasmic reticulum stress triggers autophagy. J Biol Chem 281:30299–30304. https://doi.org/10.1074/jbc.M607007200.
34. Perez-Martin M, Perez-Perez ME, Lemaire SD, Crespo JL. 2014. Oxidative stress contributes to autophagy induction in response to endoplasmic reticulum stress in *Chlamydomonas*. Plant Physiol 166:997–1008. https://doi.org/10.1104/pp.114.243659.
35. Yang X, Srivastava R, Howell SH, Bassham DC. 2016. Activation of autophagy by unfolded proteins during endoplasmic reticulum stress. Plant J 85:83–95. https://doi.org/10.1111/tpj.13091.
36. Schuck S, Gallagher CM, Walter P. 2014. ER-phagy mediates selective degradation of endoplasmic reticulum independently of the core autophagy machinery. J Cell Sci 127(Pt 18):4078–4088. https://doi.org/10.1242/jcs.154716.
37. Mesquita A, Cardenal-Munoz E, Dominguez E, Munoz-Braceras S, Nunez-Corcuera B, Phillips BA, Tabara LC, Xiong Q, Coria R, Eichinger L, Golstein P, King JS, Soldati T, Vincent O, Escalante R. 2017. Autophagy in *Dictyostelium*: mechanisms, regulation and disease in a simple biomedical model. Autophagy 13:24–40. https://doi.org/10.1080/15548627.2016.1226737.
38. Calvo-garrido J, Carilla-latorre S, Kubohara Y, Santos-rodrigo N, Mesquita A, Soldati T, Golstein P, Escalante R. 2010. Genes and pathways, cell death and infection autophagy in *Dictyostelium*. Autophagy 6:686–701. https://doi.org/10.4161/auto.6.6.12513.
39. Back S, Schröder M, Lee K, Zhang K, Kaufman RJ. 2005. ER stress signaling by regulated splicing: IRE1/HAC1/XBP1. Methods 35:395–416. https://doi.org/10.1016/j.ymeth.2005.03.001.
40. Kwolek-Mirek M, Zadrag-Tecza R. 2014. Comparison of methods used for assessing the viability and vitality of yeast cells. FEMS Yeast Res 14:1068–1079.
41. Nikawa J, Akiyoshi M, Hirata S, Fukuda T. 1996. *Saccharomyces cerevisiae* IRE2/HAC1 is involved in IRE1-mediated KAR2 expression. Nucleic Acids Res 24:4222–4226.
42. Wolf DH, Stolz A. 2012. The Cdc48 machine in endoplasmic reticulum associated protein degradation. Biochim Biophys Acta 1823:117–124. https://doi.org/10.1016/j.bbamcr.2011.09.002.
43. Arhzaouy K, Strucksberg KH, Tung SM, Tangavelou K, Stumpf M, Faix J, Schroder R, Clemen CS, Eichinger L. 2012. Heteromeric p97/p97(R155C) complexes induce dominant negative changes in wild-type and autophagy 9-deficient *Dictyostelium* strains. PLoS One 7:e46879. https://doi.org/10.1371/journal.pone.0046879.
44. Cohen NR, Knecht DA, Lodish HF. 1996. Functional expression of rat GLUT1 glucose transporter in *Dictyostelium discoideum*. Biochem J 315:971–975. https://doi.org/10.1042/bj3150971.
45. Rai M, Xiong Y, Singleton CK. 2006. Disruption of the ifkA and ifkB genes results in altered cell adhesion, morphological defects and a propensity to form pre-stalk O cells during development of *Dictyostelium*. Differentiation 74:583–595. https://doi.org/10.1111/j.1432-0436.2006.00085.x.
46. Singleton CK, Xiong Y, Kirsten JH, Pendleton KP. 2012. eIF2α kinases regulate development through the BzpR transcription factor in *Dictyostelium discoideum*. PLoS One 7:e32500. https://doi.org/10.1371/journal.pone.0032500.
47. Shamu C, Cox J, Walter P. 1994. The unfolded-protein-response pathway in yeast. Trends Cell Biol 4:56–60. https://doi.org/10.1016/0962-8924(94)90011-6.
48. Tirasophon W, Welihinda A, Kaufman R. 1998. A stress response pathway from the endoplasmic reticulum to the nucleus requires a novel bifunctional protein kinase/endoribonuclease (Ire1p) in mammalian cells. Genes Dev 12:1812–1824. https://doi.org/10.1101/gad.12.12.1812.
49. Tirasophon W, Lee K, Callaghan B, Welihinda A, Kaufman RJ. 2000. The endoribonuclease activity of mammalian IRE1 autoregulates its mRNA and is required for the unfolded protein response. Genes Dev 14:2725–2736. https://doi.org/10.1101/gad.839400.
50. Li H, Korennykh AV, Behrman SL, Walter P. 2010. Mammalian endoplasmic reticulum stress sensor IRE1 signals by dynamic clustering. Proc Natl Acad Sci U S A 107:16113–16118. https://doi.org/10.1073/pnas.1010580107.
51. Xu Z, Chikka MR, Xia H, Ready DF. 2016. Ire1 supports normal ER differentiation in developing *Drosophila* photoreceptors. J cell science 44:921–929. https://doi.org/10.1242/jcs.180406.
52. Kimmig P, Diaz M, Zheng J, Williams CC, Lang A, Aragón T, Li H, Walter P. 2012. The unfolded protein response in fission yeast modulates stability of select mRNAs to maintain protein homeostasis. Elife 1:e00048. https://doi.org/10.7554/eLife.00048.
53. Huang da W, Sherman BT, Lempicki RA. 2009. Systematic and integrative analysis of large gene lists using DAVID bioinformatics resources. Nat Protoc 4:44–57. https://doi.org/10.1038/nprot.2008.211.
54. Huang da W, Sherman BT, Lempicki RA. 2009. Bioinformatics enrichment tools: paths toward the comprehensive functional analysis of large gene lists. Nucleic Acids Res 37:1–13. https://doi.org/10.1093/nar/gkn923.
55. Mesquita A, Cardenal-Muñoz E, Dominguez E, Muñoz-Braceras S, Nuñez-Corcuera B, Phillips BA, Tábara LC, Xiong Q, Coria R, Eichinger L, Golstein P, King JS, Soldati T, Vincent O, Escalante R. 2016. Autophagy in *Dictyostelium*: mechanisms, regulation, and disease in a simple biomedical model. Autophagy 13:1–17.
56. Mesquita A, Calvo-Garrido J, Carilla-Latorre S, Escalante R. 2013. Monitoring autophagy in *Dictyostelium*. Methods Mol Biol 983:461–470. https://doi.org/10.1007/978-1-62703-302-2_26.
57. Sievers F, Wilm A, Dineen D, Gibson TJ, Karplus K, Li W, Lopez R, McWilliam H, Remmert M, Soding J, Thompson JD, Higgins DG. 2014. Fast, scalable generation of high-quality protein multiple sequence alignments using Clustal Omega. Mol Syst Biol 7:539–539. https://doi.org/10.1038/msb.2011.75.
58. Calvo-Garrido J, Carilla-Latorre S, Mesquita A, Escalante R. 2011. A proteolytic cleavage assay to monitor autophagy in *Dictyostelium discoideum*. Autophagy 7:1063–1068. https://doi.org/10.4161/auto.7.9.16629.
59. Mesquita A, Tabara LC, Martinez-Costa O, Santos-Rodrigo N, Vincent O, Escalante R. 2015. Dissecting the function of Atg1 complex in *Dictyostelium* autophagy reveals a connection with the pentose phosphate pathway enzyme transketolase. Open Biol 5:150088. https://doi.org/10.1098/rsob.150088.
60. Calvo-Garrido J, King JS, Munoz-Braceras S, Escalante R. 2014. Vmp1 regulates PtdIns3P signaling during autophagosome formation in *Dictyostelium discoideum*. Traffic 15:1235–1246. https://doi.org/10.1111/tra.12210.
61. Calvo-Garrido J, Escalante R. 2010. Autophagy dysfunction and ubiquitin-positive protein aggregates in *Dictyostelium* cells lacking Vmp1. Autophagy 6:100–109. https://doi.org/10.4161/auto.6.1.10697.
62. Dominguez-Martin E, Cardenal-Munoz E, King JS, Soldati T, Coria R, Escalante R. 2017. Methods to monitor and quantify autophagy in the social amoeba *Dictyostelium discoideum*. Cells 6:E18. https://doi.org/10.3390/cells6030018.
63. Koyama-Honda I, Itakura E, Fujiwara TK, Mizushima N. 2013. Temporal analysis of recruitment of mammalian ATG proteins to the autophagosome formation site. Autophagy 9:1491–1499. https://doi.org/10.4161/auto.25529.
64. Kishi-Itakura C, Koyama-Honda I, Itakura E, Mizushima N. 2014. Ultrastructural analysis of autophagosome organization using mammalian autophagy-deficient cells. J Cell Sci 127:4089–4102. https://doi.org/10.1242/jcs.156034.
65. Simonsen A, Stenmark H. 2008. Self-eating from an ER-associated cup. J Cell Biol 182:621–622. https://doi.org/10.1083/jcb.200807061.
66. Yoshida H, Matsui T, Yamamoto A, Okada T, Mori K. 2001. XBP1 mRNA is induced by ATF6 and spliced by IRE1 in response to ER stress to produce a highly active transcription factor. Cell 107:881–891. https://doi.org/10.1016/S0092-8674(01)00611-0.
67. Monnat J, Neuhaus EM, Pop MS, Ferrari DM, Kramer B, Soldati T. 2000. Identification of a novel saturable endoplasmic reticulum localization mechanism mediated by the C terminus of a *Dictyostelium* protein disulfide isomerase. Mol Biol Cell 11:3469–3484. https://doi.org/10.1091/mbc.11.10.3469.
68. Calvo-Garrido J, Carilla-Latorre S, La F, Egea G, Escalante R. 2008. Vacuole membrane protein 1 is an endoplasmic reticulum protein required for organelle biogenesis, protein secretion, and development. Mol Biol Cell 19:3442–3453. https://doi.org/10.1091/mbc.E08-01-0075.
69. Chow CY, Wang X, Riccardi D, Wolfner MF, Clark AG. 2015. The genetic architecture of the genome-wide transcriptional response to ER stress in the mouse. PLoS Genet 11:e1004924. https://doi.org/10.1371/journal.pgen.1004924.
70. Hooks KB, Griffiths-Jones S. 2011. Conserved RNA structures in the non-canonical Hac1/Xbp1 intron. RNA Biol 8:552–556. https://doi.org/10.4161/rna.8.4.15396.
71. Miyazaki T, Nakayama H, Nagayoshi Y, Kakeya H, Kohno S. 2013. Dissection of Ire1 functions reveals stress response mechanisms uniquely

evolved in *Candida glabrata*. PLoS Pathog 9:e1003160. https://doi.org/10.1371/journal.ppat.1003160.
72. Haze K, Yoshida H, Yanagi H, Yura T, Mori K. 1999. Mammalian transcription factor ATF6 is synthesized as a transmembrane protein and activated by proteolysis in response to endoplasmic reticulum stress. Mol Biol Cell 10:3787–3799. https://doi.org/10.1091/mbc.10.11.3787.
73. Baumeister P, Luo S, Skarnes W, Sui G, Seto E, Shi Y, Lee A. 2005. Endoplasmic reticulum stress induction of the Grp78/BiP promoter: activating mechanisms mediated by YY1 and its interactive chromatin modifiers. Mol Cell Biol 25:4529–4540. https://doi.org/10.1128/MCB.25.11.4529-4540.2005.
74. Hollien J. 2013. Evolution of the unfolded protein response. Biochim Biophys Acta 1833:2458–2463. https://doi.org/10.1016/j.bbamcr.2013.01.016.
75. Singleton CK, Xiong Y, Kirsten JH, Pendleton KP. 2012. eIF2α kinases regulate development through the BzpR transcription factor in *Dictyostelium discoideum*. PLoS One 7:e32500. https://doi.org/10.1371/journal.pone.0032500.
76. Aragon T, van Anken E, Pincus D, Serafimova IM, Korennykh AV, Rubio CA, Walter P. 2009. Messenger RNA targeting to endoplasmic reticulum stress signaling sites. Nature 457:736–740. https://doi.org/10.1038/nature07641.
77. Rubio C, Pincus D, Korennykh A, Schuck S, El-Samad H, Walter P. 2011. Homeostatic adaptation to endoplasmic reticulum stress depends on Ire1 kinase activity. J Cell Biol 193:171–184. https://doi.org/10.1083/jcb.201007077.
78. Ding WX, Ni HM, Gao W, Hou YF, Melan MA, Chen X, Stolz DB, Shao ZM, Yin XM. 2007. Differential effects of endoplasmic reticulum stress-induced autophagy on cell survival. J Biol Chem 282:4702–4710. https://doi.org/10.1074/jbc.M609267200.
79. Fouillet A, Levet C, Virgone A, Robin M, Dourlen P, Rieusset J, Belaidi E, Ovize M, Touret M, Nataf S, Mollereau B. 2012. ER stress inhibits neuronal death by promoting autophagy. Autophagy 8:915–926. https://doi.org/10.4161/auto.19716.
80. Velentzas PD, Velentzas AD, Mpakou VE, Antonelou MH, Margaritis LH, Papassideri IS, Stravopodis DJ. 2013. Detrimental effects of proteasome inhibition activity in *Drosophila melanogaster*: implication of ER stress, autophagy, and apoptosis. Cell Biol Toxicol 29:13–37. https://doi.org/10.1007/s10565-012-9235-9.
81. Pankiv S, Clausen TH, Lamark T, Brech A, Bruun JA, Outzen H, Øvervatn A, Bjørkøy G, Johansen T. 2007. p62/SQSTM1 binds directly to Atg8/LC3 to facilitate degradation of ubiquitinated protein aggregates by autophagy. J Biol Chem 282:24131–24145. https://doi.org/10.1074/jbc.M702824200.
82. Tabara LC, Escalante R. 2016. VMP1 establishes ER-microdomains that regulate membrane contact sites and autophagy. PLoS One 11:e0166499. https://doi.org/10.1371/journal.pone.0166499.
83. Axe EL, Walker SA, Manifava M, Chandra P, Roderick HL, Habermann A, Griffiths G, Ktistakis NT. 2008. Autophagosome formation from membrane compartments enriched in phosphatidylinositol 3-phosphate and dynamically connected to the endoplasmic reticulum. J Cell Biol 182:685–701. https://doi.org/10.1083/jcb.200803137.
84. Gaudet P, Pilcher KE, Fey P, Chisholm RL. 2007. Transformation of *Dictyostelium discoideum* with plasmid DNA. Nat Protoc 2:1317–1324. https://doi.org/10.1038/nprot.2007.179.
85. Veltman DM, Akar G, Bosgraaf L, Van Haastert PJ. 2009. A new set of small, extrachromosomal expression vectors for *Dictyostelium discoideum*. Plasmid 61:110–118. https://doi.org/10.1016/j.plasmid.2008.11.003.
86. Kunkel TA. 1985. Rapid and efficient site-specific mutagenesis without phenotypic selection. Proc Natl Acad Sci U S A 82:488–492. https://doi.org/10.1073/pnas.82.2.488.
87. Adachi H, Hasebe T, Yoshinaga K, Ohta T, Sutoh K. 1994. Isolation of *Dictyostelium discoideum* cytokinesis mutants by restriction enzyme-mediated integration of the blasticidin S resistance marker. Biochem Biophys Res Commun 205:1808–1814. https://doi.org/10.1006/bbrc.1994.2880.
88. Trapnell C, Roberts A, Goff L, Pertea G, Kim D, Kelley DR, Pimentel H, Salzberg SL, Rinn JL, Pachter L. 2012. Differential gene and transcript expression analysis of RNA-seq experiments with TopHat and Cufflinks. Nat Protoc 7:562–578. https://doi.org/10.1038/nprot.2012.016.
89. Parikh A, Miranda ER, Katoh-Kurasawa M, Fuller D, Rot G, Zagar L, Curk T, Sucgang R, Chen R, Zupan B, Loomis WF, Kuspa A, Shaulsky G. 2010. Conserved developmental transcriptomes in evolutionarily divergent species. Genome Biol 11:R35. https://doi.org/10.1186/gb-2010-11-3-r35.
90. Fey P, Dodson RJ, Basu S, Chisholm RL. 2013. One stop shop for everything *Dictyostelium*: dictyBase and the Dicty Stock Center in 2012. Methods Mol Biol 983:59–92. https://doi.org/10.1007/978-1-62703-302-2_4.
91. Consortium TU. 2008. The universal protein resource (UniProt). Nucleic Acids Res 36:D190–D195. https://doi.org/10.1093/nar/gkm895.
92. Huang X, Miller W. 1991. A time-efficient, linear-space local similarity algorithm. Adv Appl Math 12:337–357. https://doi.org/10.1016/0196-8858(91)90017-D.
93. Duret L, Gasteiger E, Perriere G. 1996. LALNVIEW: a graphical viewer for pairwise sequence alignments. Comput Appl Biosci 12:507–510.
94. Mi H, Muruganujan A, Thomas PD. 2013. PANTHER in 2013: modeling the evolution of gene function, and other gene attributes, in the context of phylogenetic trees. Nucleic Acids Res 41(Database Issue):D377–D386. https://doi.org/10.1093/nar/gks1118.
95. Davidson AJ, King JS, Insall RH. 2013. The use of streptavidin conjugates as immunoblot loading controls and mitochondrial markers for use with *Dictyostelium discoideum*. Biotechniques 55:39–41. https://doi.org/10.2144/000114054.